RESTRICTED CLASSIFIED COPY NO. 112
RM No. E8F09e

Inactive
Auth. J. W. Crowley 3/25/54
per change 1702 MHA 4/1/54

RESEARCH MEMORANDUM

ALTITUDE-WIND-TUNNEL INVESTIGATION OF A 4000-POUND-THRUST AXIAL-FLOW TURBOJET ENGINE

VI - COMBUSTION-CHAMBER PERFORMANCE

By I. Irving Pinkel and Harold Shames

Flight Propulsion Research Laboratory
Cleveland, Ohio

CLASSIFICATION CANCELLED

Authority J. W. Crowley Date 12/7/53
(E.O. 10501)
By MHA 12/18/53 See NACA R 7 1702

CLASSIFIED DOCUMENT

This document contains classified information affecting the National Defense of the United States within the meaning of the Espionage Act, USC 50:31 and 32. Its transmission or the revelation of its contents in any manner to an unauthorized person is prohibited by law. Information so classified may be imparted only to persons in the military and naval services of the United States, appropriate civilian officers and employees of the Federal Government who have a legitimate interest therein, and to United States citizens of known loyalty and discretion who of necessity must be informed thereof.

LIBRARY COPY
DEC 17 1953
LANGLEY AERONAUTICAL LABORATORY
LIBRARY, NACA
LANGLEY FIELD, VIRGINIA

NATIONAL ADVISORY COMMITTEE
FOR AERONAUTICS
WASHINGTON
August 4, 1948

RESTRICTED

UNCLASSIFIED

3 1176 01435 5367

UNCLASSIFIED

 RESTRICTED

NATIONAL ADVISORY COMMITTEE FOR AERONAUTICS

RESEARCH MEMORANDUM

ALTITUDE-WIND-TUNNEL INVESTIGATION OF A 4000-POUND-THRUST AXIAL-FLOW TURBOJET ENGINE

VI - COMBUSTION-CHAMBER PERFORMANCE

By I. Irving Pinkel and Harold Shames

SUMMARY

An analysis of the performance of the types A, B, and C combustion chambers of the 4000-pound-thrust axial-flow turbojet engine is presented. The data were obtained from investigations of the complete engine over a range of pressure altitudes from 5000 to 40,000 feet and ram pressure ratios from 1.00 to 1.86. The combustion-chamber pressure losses, the effect of the losses on cycle efficiency, and the combustion efficiency are discussed.

The type A combustion chamber had the highest over-all (total) pressure loss and the type C the lowest, of the three combustion chambers investigated when used under equivalent engine configurations and operating conditions. Pressure losses due to friction were highest for the type A and lowest for the type C combustion chamber; pressure losses due to heat addition to the air flowing in the combustion chamber were highest for type C and lowest for type A. The variation with altitude of the ratios of the pressure losses due to heat addition and those due to friction to the combustion-chamber inlet total pressure, called the momentum and friction pressure-loss ratios, respectively, was negligible for the type A combustion chamber. The data for the type B combustion chamber showed that the friction pressure-loss ratio increased, and the momentum pressure-loss ratio decreased, with increasing ram pressure ratio.

The loss in cycle efficiency due to the pressure losses in the combustion chamber was found to be of little consequence in the design operating range of the engine. At low engine speeds, however, this loss in cycle efficiency can be as large as 50 percent of the cycle efficiency attained.

The data taken at static conditions and a pressure altitude of 5000 feet show the type B combustion chamber to have the highest

RESTRICTED

UNCLASSIFIED

and the type A the lowest combustion efficiency. The combustion efficiency improved with engine speed and ram pressure ratio at all altitudes and decreased with increasing altitude. At rated engine speed the altitude effect on combustion efficiency was no greater than 5 percent for the range of pressure altitudes investigated.

INTRODUCTION

A study of the performance of the components of 4000-pound-thrust axial-flow turbojet engine has been conducted in the Cleveland altitude wind tunnel. An analysis of the performance of the combustion chamber based on data obtained with the complete engine is presented. A discussion of performance and operational characteristics of the complete engine is given in references 1 to 3 and an analysis of the compressor and the turbine performance is given in references 4 and 5, respectively.

The working substances of the work cycle in jet-propulsion engines are the materials involved in the combustion. For this reason the flow characteristics of the combustion chamber and the manner of heat release influence the over-all performance of the jet engine. The combustion of the fuel should be completed before the gases reach the turbine and the loss in total pressure of the gas flow through the combustion chamber should be low compared with the difference between the compressor-outlet total pressure and the free-stream static pressure. If combustion is incomplete, not only is fuel lost but also the fuel that is unconsumed in the combustion chamber may burn on the surface of the turbine blades and raise the turbine-blade temperature above safe limits. The loss in total pressure through the combustion chamber reduces the cycle efficiency and the mass flow of air through the engine.

The variation with simulated flight conditions of the pressure losses through the combustion chamber, of the loss in engine cycle efficiency that results from these pressure losses, and of the combustion-chamber efficiency are discussed for the types A, B, and C combustion chambers. These combustion-chamber types represent the standard combustion chamber (type A) and two modifications. The pressure losses due to fluid friction and to the addition of heat to the flowing gas in the combustion chamber are separately evaluated by means of a pressure-loss chart developed in reference 6. The combustion efficiency of the combustion chamber of the axial-flow-type turbojet engine investigated is correlated with the temperature of the gas at the combustion-chamber outlet.

The engine operating range for which data are discussed extended from pressure altitudes of 5000 to 40,000 feet and ram

654

pressure ratios from 1.00 to 1.86. The ram pressure ratio is defined as the ratio of the total pressure at the engine inlet to the tunnel static pressure. The data for this range are necessarily restricted to the operable engine speeds at each pressure altitude and ram pressure ratio and are not sufficiently complete to determine the altitude limits of operation of the three combustion chambers used in this investigation.

The high-flow compressor represents no engine modification contemplated for production by the engine manufacturer but represents the attempt of the engine manufacturer to obtain increased performance by modifying the standard 4000-pound-thrust axial-flow turbojet engine at the time of this investigation.

DESCRIPTION OF COMBUSTION CHAMBERS

The three combustion chambers are illustrated in figure 1. Each chamber consists of an outer duct and a liner (sometimes referred to as a "basket"). All the chambers have the same dimensions and differ only in the primary-air entrance arrangements on the liner dome. In the type A combustion chamber (fig. 1), standard for the engine investigated, all the louvers shown in the dome are pushed out. In the type B combustion chamber, the middle row of louvers is pushed in to give an upstream-velocity component to the air on the inside surface of the dome and thus improve the engine starting characteristics. The type C combustion chamber has fewer louvers, which are pushed in. The dome is surrounded by a ram hood. Swirling of the air inside the dome of the type C combustion chamber is accomplished by two rows of louvers arranged to induce circumferential air flow in opposite directions. Type C was designed to raise the upper blow-out limit for high-altitude operation. The blow-out limits and the starting characteristics of the three types of combustion chamber are discussed in reference 2.

The turbojet engine has eight combustion chambers arranged in parallel. Each combustion chamber is fitted with inlet and outlet ducts leading to the compressor outlet and turbine inlet, respectively.

ENGINE INSTALLATION AND INSTRUMENTATION

A complete description of the installation and instrumentation of the 4000-pound-thrust axial-flow turbojet engine in the Cleveland altitude wind tunnel is given in reference 1; the description pertinent to this report is included herein.

The engine was rigidly suspended from a 7-foot-chord wing mounted in the test section of the tunnel (fig. 2). For the static runs, a cowling was fitted to the engine inlet and the engine air was drawn from the tunnel. For the runs that simulated flight conditions, air was supplied to the engine inlet by a duct connected to the tunnel make-up air supply. Inlet-air pressure up to approximately sea-level atmosphere could be maintained at all pressure altitudes corresponding to the desired ram pressure ratio (ratio of engine-inlet total pressure to tunnel static pressure) to be simulated. At a pressure altitude of 40,000 feet, ram pressure ratios as high as 1.86 were attained by this means. Although refrigerated air was used, the cooling capacity of the system was insufficient to maintain NACA standard temperatures at the engine inlet for the low ram pressure ratios at the high altitudes. At pressure altitudes above 30,000 feet, the engine inlet-air temperatures were usually higher than those required by the simulated flight conditions in standard NACA air.

The stations at which pressure probes and thermocouples were installed are shown in figure 3. The instrumentation at the inlet and the outlet of the combustion chamber, stations 4 and 5, is pertinent to this report.

The arrangement of thermocouples and total-pressure probes at the compressor outlet, taken as the combustion-chamber inlet, is shown in figure 4. Two separate sets of total-pressure probes were used. The NACA set consisted of three probes mounted on rakes lying on radii that bisect the compressor outlets. The other probes were single total-pressure probes displaced circumferentially from these radii in the same compressor outlet. Two exposed thermocouples were installed with each set of NACA total-pressure probes. Four of the eight compressor outlets were so instrumented. The total pressure at the turbine inlet was obtained with two diametrically opposite total-pressure probes located on the leading edge of the turbine-nozzle vane at the mean radius of the turbine-nozzle annulus. No thermocouples were placed at the entrance to the turbine nozzle. The turbine-inlet total temperature was computed from the total temperature of the gases in the tail pipe.

Pressures were measured by mercury manometers with the tunnel static pressure used as the reference pressure. The manometers were read to ±0.05 inch of mercury, which is equivalent to a maximum reading error of ±3.6 pounds per square foot. An error of 7.2 pounds per square foot is possible in computing the difference in the total pressure of the flow from compressor outlet to turbine inlet. For low air mass flows through the engine, this error is sometimes 25 percent of the measured pressure drop across the combustion chamber.

654

The types A, B, and C combustion chambers were installed in configurations of the turbojet engine shown in the following table:

Combustion chamber	Compressor	Turbine-nozzle area (sq in.)	Tail-pipe-nozzle diameter (in.)
A	Low flow	Small, 101.9-97.7	$16\frac{1}{4}$
B	Low flow	Standard, 106.8-108.0	$16\frac{3}{4}$
C	High flow	Large, 121.0-119.9	18

Because of the different engine configurations used with each combustion-chamber type a direct comparison of performance among combustion chambers was sometimes impossible.

SYMBOLS

The following symbols are used in the analysis:

A area of equivalent combustion chamber of constant cross section, square feet

C constant, p/ρ^{γ}

c_p specific heat at constant pressure, Btu per pound $^{\circ}R$

$c_{p,b}$ average specific heat at constant pressure for combustion chamber, Btu per pound $^{\circ}R$

$c_{p,c}$ average specific heat at constant pressure for compressor, Btu per pound $^{\circ}R$

$c_{p,j}$ average specific heat at constant pressure from station 9 to station 0, Btu per pound $^{\circ}R$

$c_{p,t}$ average specific heat at constant pressure for turbine, Btu per pound $^{\circ}R$

g mass ratio, 32.2 pounds mass per slug

h lower heating value of fuel, Btu per pound, (18,600)

J mechanical equivalent of heat, foot-pounds per Btu, (778)

K combustion-chamber friction pressure-loss factor

M Mach number, ratio of gas speed to local speed of sound

N engine rotational speed, rpm

P total pressure, pounds per square foot absolute

ΔP_F loss in total pressure due to friction, pounds per square foot

ΔP_M loss in total pressure due to heat additions to the gas in the combustion chamber (so-called momentum pressure loss), pounds per square foot

ΔP_T over-all loss in total pressure due to friction and momentum changes, pounds per square foot

p static pressure, pounds per square foot absolute

R gas constant for air, foot-pounds per pound $^{\circ}R$, (53.3)

T total temperature, $^{\circ}R$

T_i indicated temperature, $^{\circ}R$

t static temperature, $^{\circ}R$

W air mass flow through each combustion chamber, pounds per second

W_a air mass flow through entire engine, pounds per second

W_f fuel mass flow, pounds per second

W_g gas mass flow through entire engine, pounds per second

γ ratio of specific heat at constant pressure to specific heat at constant volume

η engine cycle efficiency

$\Delta\eta$ engine cycle-efficiency loss

654

η_b combustion-chamber efficiency

η_t turbine adiabatic efficiency

θ_2 ratio of compressor inlet-air total temperature to NACA standard sea-level static temperature

ρ air density, pounds per cubic foot

ρ_T air density, measured under stagnation conditions, pounds per cubic foot

Subscripts:

0 free stream

1 entrance to engine diffuser

4 combustion-chamber inlet; also compressor outlet

5 combustion-chamber outlet; also turbine inlet

6 turbine outlet

8 tail rake

9 vena contracta in jet issuing from tail-pipe nozzle

B entrance to combustion zone of equivalent combustion chamber (station B)

c compressor

t turbine

METHODS OF ANALYSIS

Loss in total pressure across combustion chamber. - The measured loss in total pressure across the combustion chamber was subject to appreciable error because it was computed by taking the difference in readings of separate mercury manometers connected to the compressor-outlet and turbine-inlet total-pressure tubes. The NACA instrumentation at the compressor outlet (fig. 4) gave substantially the same readings as the other instrumentation, but the small differences in readings obtained with the two sets of instrumentation gave differences in combustion-chamber pressure losses as great as 50 percent.

The turbine-inlet total pressure was obtained at two points in the turbine-nozzle diaphragm annulus. These two pressure measurements were insufficient to give an accurate representative reading of the total pressure at the turbine inlet.

Because of the uncertainties in the pressure-loss data, the pressure-loss chart developed in reference 6 was used to aid in determining which set of instrumentation was giving pressure-loss values closer to the correct values. The chart is reproduced as figure 5. This chart also provides a means of separately determining that part of the pressure loss due to flow losses involving friction ΔP_F and that part of the pressure loss due to the addition of heat to the air stream ΔP_M. The chart permits the pressure-loss characteristics of the combustion chamber to be specified by a friction pressure-loss factor K related to the friction pressure-loss characteristics and by an equivalent area A related to the momentum pressure-loss characteristics of the combustion chamber. The friction pressure-loss factor is defined by the equation

$$\Delta P_F = K \frac{W^2 R T_4}{P_4} \tag{1}$$

The equivalent area A is the cross section of a corresponding combustion chamber of constant cross-sectional area having the same momentum pressure-loss characteristics as the actual combustion chamber. The over-all pressure loss across the combustion chamber is $\Delta P_T = \Delta P_F + \Delta P_M$. A résumé of the use and applications of the pressure-loss chart is given in appendix A.

Cycle efficiency. - The cycle efficiency was determined according to the standard definition; that is,

$$\eta = \frac{\text{heat supplied by source - heat rejected to sink}}{\text{heat supplied by source}}$$

$$= \frac{c_{p,b}\,(T_5 - T_4) - c_{p,j}\,(t_9 - t_0)}{c_{p,b}\,(T_5 - T_4)}$$

The expression for the loss in cycle efficiency due to the pressure losses in the combustion chamber is developed in appendix B (equation (B6)) as

$$\Delta\eta = \frac{c_{p,j}t_9\left[1 - \left(\frac{P_5}{P_4}\right)^{\frac{\gamma-1}{\gamma}}\right]}{c_{p,b}\,(T_5 - T_4)}$$

where γ is the average value between stations 5 and 9. This expression is approximate because of the assumptions made in its development.

Combustion-chamber efficiency. - The combustion-chamber efficiency is defined as the ratio of the actual enthalpy rise across the combustion chamber of the gases with an average specific heat to the theoretical enthalpy rise that would be realized with complete combustion; that is,

$$\eta_b = \frac{c_{p,b}\,(T_5 - T_4)}{(W_f/W_a)h}$$

No correction was made for heat losses from the combustion chamber.

Greatly simplified considerations involving the kinetics of the combustion reaction and the reaction time available in the combustion chamber indicated the possibility of plotting log $\eta\sqrt{T_5}$ against $1/T_5$ as straight lines for constant values of the parameter P_4/W^2. Combustion efficiency was so plotted for the type B combustion chamber.

METHODS OF CALCULATION

Determination of air flow. - The air flow through the combustion chambers was determined from the temperature and pressure measurements obtained with the survey rake placed at the outlet of the tail-pipe nozzle (station 8, fig. 3) by

$$W_g = \frac{p_8A_8}{R}\sqrt{\frac{2Jgc_{p,8}}{t_8}\left[\left(\frac{P_8}{p_8}\right)^{\frac{\gamma_8-1}{\gamma_8}} - 1\right]}$$

$$W_a = W_g - W_f$$

Inasmuch as the turbojet engine investigated has eight combustion chambers, the air flow per combustion chamber W is equal to $W_a/8$.

Determination of temperatures. - Static temperatures were calculated from indicated temperature readings by

$$t = \frac{T_1}{1 + \alpha\left[\left(\frac{P}{p}\right)^{\frac{\gamma-1}{\gamma}} - 1\right]}$$

where α is the thermocouple impact-recovery factor taken as 0.85, based on the calibration of the type of exposed thermocouple used in this investigation.

The total temperature was obtained from the isentropic adiabatic relation

$$\frac{T}{t} = \left(\frac{P}{p}\right)^{\frac{\gamma-1}{\gamma}}$$

Determination of combustion-chamber outlet total temperature. - The combustion-chamber outlet total temperature T_5 was computed from the rake temperature T_8 by

$$T_5 = \Delta T_t + T_6$$

The total temperature at the turbine outlet T_6 was considered to be equal to the total temperature at the tail rake T_8. Based on the assumption that the measured enthalpy rise across the compressor $c_{p,c}\Delta T_c$ is equal to the enthalpy drop across the turbine $c_{p,t}\Delta T_t$ and $W_a = W_g$, the value of ΔT_t is

$$\Delta T_t = \frac{c_{p,c}\Delta T_c}{c_{p,t}}$$

The expression for T_5 is then

$$T_5 = \frac{c_{p,c}\Delta T_c}{c_{p,t}} + T_8$$

654

No correction was made for mechanical-friction losses that would give slightly higher values for ΔT_t and T_5 than were computed from the preceding equations.

Determination of ambient gas temperatures at engine inlet and outlet. - The engine inlet-air temperature that corresponds to ram pressure ratio and pressure altitude could not be maintained for all of the runs. The calculated ambient temperature t_0 that corresponds to the engine inlet conditions was computed from the isentropic relation

$$t_0 = T_1 \left(\frac{p_0}{p_1}\right)^{\frac{\gamma_0 - 1}{\gamma_0}}$$

Because the tail-rake static pressure p_8 is generally greater than the tunnel ambient pressure p_0, the temperature of the exhaust gases t_9 at the ambient tunnel pressure was similarly computed

$$t_9 = t_8 \left(\frac{p_0}{p_8}\right)^{\frac{\gamma_8 - 1}{\gamma_8}}$$

EXPERIMENTAL RANGE

The combustion-chamber data discussed are restricted to the operable range of engine speeds that correspond to the pressure altitudes and ram pressure ratios investigated. Data with the type A and type C combustion chambers were taken only for the static case over an altitude range from 5000 to 40,000 feet; all comparisons among combustion chambers are therefore limited to this case. Data for the type B combustion chamber were taken at pressure altitudes of 5000 and 40,000 feet for the static case and at 30,000 and 40,000 feet for ram pressure ratios ranging from 1.10 to 1.86. At a ram pressure ratio of 1.20, data were available to compute the type B combustion-chamber efficiency over a range of pressure altitudes from 10,000 to 40,000 feet.

RESULTS AND DISCUSSION

Combustion-Chamber Pressure Losses

A comparison of the experimentally determined over-all (total) pressure-loss ratios $\Delta P_T/P_4$ with those obtained from the pressure-loss chart for the types A, B, and C combustion chambers at pressure altitudes from 5000 to 40,000 feet under static conditions is shown in figure 6. A similar comparison is given in figure 7 for the type B combustion chamber operating at pressure altitudes of 30,000 and 40,000 feet with the ram pressure ratio ranging from 1.10 to 1.86. The corresponding values of the friction pressure-loss ratios $\Delta P_F/P_4$ and the momentum pressure-loss ratios $\Delta P_M/P_4$ obtained from the pressure-loss chart are included in figures 6 and 7. In general, the values of the over-all pressure-loss ratios obtained from the chart lie between the values obtained with the NACA and the commercial instrumentation. The values of the friction pressure-loss factor K and the equivalent area of cross section A used to obtain the pressure-loss ratios from the chart are given in the following table. The methods used to obtain the values of K and A are discussed in appendix A.

Combustion chamber	K	A (sq ft) (a)	KA^2
A	0.667	0.30	0.060
B[b]	.432	.25	.027
B[c]	.447	.25	.028
C	.347	.24	.020

[a]Actual liner cross-sectional area is approximately 0.30 square foot.

[b]Results obtained with friction and over-all pressure-loss data (fig. 20(a), appendix A).

[c]Results obtained only with over-all pressure-loss data (fig. 20(b), appendix A).

The large difference in the values of KA^2 for the types A and B combustion chambers appears to be excessive in view of the small difference in liner-dome arrangement involved. In figure 6, however, the values of the over-all pressure-loss ratios predicted

654

from the chart with the values of KA^2 given for the three types of combustion chamber are shown to agree with the measured values within the limits of experimental error.

The curves plotted in figures 6 and 7 are regrouped in subsequent figures to provide comparisons and to indicate the trends in the data.

In order to make the comparison of the pressure losses for types A, B, and C combustion chambers shown in figure 8, the pressure losses for types B and C were computed by means of the pressure-loss chart. This method of comparison was required because the engine configuration differed for each combustion chamber. The computation of pressure losses was based on the assumption that the types B and C combustion chambers were installed in an engine with the same components used with the type A combustion chamber. The data for type A were obtained with the low-flow compressor, the small turbine nozzle, and the $16\frac{1}{4}$-inch-diameter tailpipe nozzle for static conditions.

The type of combustion chamber with the lowest value of cross-sectional area of the equivalent combustion chamber A has the highest value of momentum pressure loss for a given value of generalized air mass flow $W\sqrt{T_4}/P_4$ and temperature ratio T_5/T_4. The type C combustion chamber would therefore have the highest momentum pressure losses and type A the lowest. This relative order of the momentum pressure-loss values is shown in figure 8, in which the calculated momentum pressure-loss ratio $\Delta P_M/P_B$ for all combustion chambers is plotted against the corrected engine speed $N/\sqrt{\theta_2}$ for pressure altitudes of 10,000 and 30,000 feet for the static conditions.

The friction pressure loss increases with the value of K. According to the listed values of K, the friction pressure-loss ratio $\Delta P_F/P_4$ should be highest for the type A combustion chamber and lowest for type C. The order of the relative values of $\Delta P_F/P_4$ for the combustion chambers is indicated by the relative values of K. The calculated friction pressure-loss values for all combustion chambers are also shown in figure 8. A comparison of the data in figures 8(a) and 8(b) shows that $\Delta P_F/P_4$ is greater than $\Delta P_M/P_B$ for types A and B combustion chambers for all values of the corrected engine speed $N/\sqrt{\theta_2}$. For the type C combustion chamber, $\Delta P_M/P_B$ is approximately equal to $\Delta P_F/P_4$ for all values of $N/\sqrt{\theta_2}$

at pressure altitudes of 10,000 and 30,000 feet. The computed over-all (total) pressure-loss ratio $\Delta P_T/P_4$, also plotted in figures 8(a) and 8(b), is highest for type A and lowest for the type C combustion chamber for both altitudes.

The values of $\Delta P_T/P_4$, $\Delta P_F/P_4$, and $\Delta P_M/P_B$ are given in figure 9 for the type B combustion chamber at a pressure altitude of 30,000 feet with values of ram pressure ratio ranging from 1.10 to 1.76. The largest effect of ram pressure ratio on the friction pressure-loss ratio occurred between a ram pressure ratio of 1.20 and 1.65. In general, the over-all and friction pressure-loss ratios increase and the momentum pressure-loss ratio decreases with ram pressure ratio. The increase in $\Delta P_F/P_4$ is due to the large $W\sqrt{T_4}/P_4$ at the high ram pressure ratios and the decrease in $\Delta P_M/P_4$ is attributed to the small temperature ratio required to maintain a given engine speed at high ram pressure ratios.

Plots of $\Delta P_T/P_4$, $\Delta P_F/P_4$, and $\Delta P_M/P_B$ are given in figure 10 for the type A combustion chamber for static conditions at pressure altitudes ranging from 5000 to 40,000 feet. The curves show that the effect of altitude on all the pressure-loss ratios is negligible for the engine configuration with the low-flow compressor, the small turbine nozzle, and the $16\frac{1}{4}$-inch-diameter tail-pipe nozzle.

Cycle-Efficiency Losses

The expression developed in appendix B for the loss in cycle efficiency $\Delta\eta$ can be considered only approximate because of the assumptions made in the development: that the engine speed and the temperature rise across the combustion chamber are the same for the cases with or without combustion-chamber pressure losses.

The cycle-efficiency losses that result from combustion-chamber pressure losses are shown for the types A, B, and C combustion chambers in figure 11 for static conditions with altitudes ranging from 5000 to 40,000 feet, and in figure 12 for the type B combustion chamber at an altitude of 40,000 feet with the ram pressure ratio ranging from 1.20 to 1.86. The data are presented as the fractional cycle-efficiency loss $\Delta\eta/\eta$. The values of the corresponding cycle efficiency η are plotted for reference. At the low corrected engine speeds the loss in cycle efficiency represents as much as one-half the efficiency obtained. The fractional cycle-efficiency loss varied inversely with corrected engine speed.

Above a corrected engine speed of 7600 rpm, the fractional cycle-efficiency losses are no greater than 0.06 for any combustion chamber.

The effect of altitude on $\Delta\eta/\eta$ for the type A combustion chamber is shown in figure 13 replotted from data given in figure 11 for static conditions at pressure altitudes ranging from 5000 to 40,000 feet. The fractional cycle-efficiency losses increase with pressure altitude (except at 30,000 ft) for values of the corrected engine speed less than 6500 rpm. The curve for a pressure altitude of 30,000 feet varies from the general trend. At a corrected engine speed of 5750 rpm, the value of $\Delta\eta/\eta$ at 40,000 feet is 1.6 the value at 5000 feet. In the neighborhood of the design engine speed (7600 rpm) the effect of altitude on $\Delta\eta/\eta$ is poorly defined in figure 13.

The effect of ram pressure ratio on $\Delta\eta/\eta$ at a pressure altitude of 40,000 feet is shown in figure 14 replotted from data given in figure 12 for the type B combustion chamber. The value of $\Delta\eta/\eta$ decreases with increasing ram pressure ratio for the entire range of corrected engine speed. At a corrected engine speed of 6250 rpm, the value of $\Delta\eta/\eta$ for a ram pressure ratio of 1.20 is 1.7 the value for a ram pressure ratio of 1.62.

High cycle-efficiency losses contributed to engine-acceleration difficulties encountered in operation at low engine speeds. The high cycle-efficiency losses require a larger temperature rise across the combustion chamber to provide the energy to accelerate the engine than would be needed without these losses. At starting engine speed the combustion efficiency is quite low. Under these conditions, large increases in the fuel-air ratio are required to obtain the necessary temperature rise across the combustion chamber. As a result, high cycle-efficiency losses require that the combustion chamber operate in the range of fuel-air ratios where the combustion-chamber efficiency falls rapidly with increasing fuel-air ratio.

Combustion Efficiency

The combustion efficiency η_b is plotted against the corrected engine speed $N/\sqrt{\theta_2}$ for the types A, B, and C combustion chambers in figure 15. These data show that, at a pressure altitude of 5000 feet and for static conditions, the combustion efficiency of all the combustion chambers increased with corrected engine speed. The combustion efficiency was highest for the type B combustion chamber and lowest for type A.

The effect of pressure altitude on the combustion efficiency of the type B combustion chamber at a ram pressure ratio of 1.20 is shown in figure 16. Combustion efficiency decreased with increasing altitude over the entire range of corrected engine speeds. The variations in combustion efficiency with pressure altitude for the type B combustion chamber are shown to decrease with increasing corrected engine speed.

The variation of combustion efficiency with ram pressure ratio is shown in figure 17 for the type B combustion chamber at a pressure altitude of 40,000 feet. The combustion efficiency improved with ram pressure ratio over the entire range of corrected engine speeds. The improvement obtained at the high ram pressure ratios was greatest in the low range of corrected engine speeds.

A method of correlating combustion efficiency is presented in figure 18. Log $\eta_b\sqrt{T_5}$ is plotted against $1/T_5$ for the type B combustion chamber. Points representing constant values of the parameter P_4/W^2 for a range of engine conditions determine a single straight line. The points on this figure were obtained from cross plots of $\eta\sqrt{T_5}$ against P_4/W^2 and $1/T_5$ against P_4/W^2. Charts of this type are useful in obtaining an estimate of the combustion efficiencies beyond the value of T_5 covered by experiment because the direction of extrapolation is well defined by straight lines. Extrapolation should not be made to a set of combustion-chamber conditions for which there is reason to believe that the location of the origin of the flame changes.

SUMMARY OF RESULTS

The following results were obtained for types A, B, and C combustion chambers operating in the complete 4000-pound-thrust axial-flow turbojet engine at static conditions over a range of pressure altitudes from 5000 to 40,000 feet and for the type B combustion chamber at ram pressure ratios from 1.00 to 1.86 and the same pressure altitudes:

1. From the measured pressure-loss data, the following values of the friction pressure-loss coefficient K and the cross-sectional area of the equivalent combustion chamber A were obtained:

Combustion chamber	K	A (sq ft)	KA^2
A	0.667	0.30	0.060
B	.432	.25	.027
C	.347	.24	.020

By means of the pressure-loss chart and these values of K and A, which define the pressure-loss characteristics of the combustion chambers, the following conclusions regarding the pressure losses of the types A, B, and C combustion chambers are drawn.

(a) For the same values of the corrected engine speed $N/\sqrt{\theta_2}$, the combustion-chamber momentum pressure-loss (that is, loss due to heat addition to gas flowing in combustion chamber) ratio $\Delta P_M/P_B$ obtained by means of the pressure-loss chart was highest for the type C combustion chamber and lowest for the type A combustion chamber. For types A and B the friction pressure-loss ratio was always greater than the corresponding momentum pressure-loss ratio. For the type C combustion chamber the momentum pressure-loss ratio was approximately equal to the friction pressure-loss ratio over the entire range of corrected engine speeds at pressure altitudes of 10,000 and 30,000 feet.

(b) For the same values of the corrected engine speed, the friction pressure-loss ratio $\Delta P_F/P_4$ was highest for the type A combustion chamber and lowest for the type C combustion chamber.

(c) The over-all pressure-loss ratio $\Delta P_T/P_4$ was highest for the type A combustion chamber and lowest for type C at all pressure altitudes for the static case.

(d) For the type A combustion chamber used with the low-flow compressor, the small turbine nozzles, and the $16\frac{1}{4}$-inch-diameter tail pipe, the combustion-chamber momentum, friction, and over-all (total) pressure-loss ratios were only slightly affected by variations in pressure altitude for the same values of the corrected engine speed.

(e) The friction and the over-all pressure-loss ratios increased with ram pressure ratio and the momentum pressure loss decreased with increasing ram pressure ratio for the type B combustion chamber.

2. The fractional cycle-efficiency loss $\Delta\eta/\eta$ due to combustion-chamber pressure losses varied inversely with corrected engine speed.

The value of $\Delta\eta/\eta$ increased with pressure altitude and decreased with increasing ram pressure ratio. The loss in cycle efficiency due to combustion-chamber pressure losses was negligible in the design operating range of the engine, but at low engine speeds was as high as 50 percent of the efficiency attained.

3. The data taken at static conditions and a pressure altitude of 5000 feet indicate that the type B combustion chamber had the highest combustion efficiency and type A the lowest. The combustion efficiency generally increased with corrected engine speed and ram pressure ratio and decreased with increasing pressure altitude. At the rated engine speed the altitude effect on combustion efficiency was no greater than 5 percent for the range of pressure altitudes investigated.

4. In the range of the data discussed, straight lines were obtained when $\log \eta_b T_5$ was plotted against $1/T_5$ for constant values of the parameter P_4/W^2, where η_b is combustion-chamber efficiency, T_5 is turbine-inlet total temperature, P_4 is compressor-outlet pressure and W is air flow through one combustion chamber. Such plots are useful for predicting approximate combustion efficiencies for operating conditions beyond the limits of the data.

Flight Propulsion Research Laboratory,
National Advisory Committee for Aeronautics,
Cleveland, Ohio.

APPENDIX A

PRESSURE-LOSS CHART

The development and use of the combustion-chamber pressure-loss chart described in reference 6 is summarized.

Development of chart. - The following assumptions were made to derive the equations on which the combustion-chamber pressure-loss chart is based:

1. The actual combustion-chamber pressure losses can be matched by those of an equivalent combustion chamber of uniform cross-sectional area A having the form shown in figure 19.

2. The over-all loss in total pressure ΔP_T is equal to the sum of the pressure loss across the combustion chamber with the air flowing and no combustion occurring (engine windmilling) ΔP_F plus the pressure loss due to heat addition to the air flow in the combustion chamber, or the so-called momentum pressure loss, ΔP_M; that is,

$$\Delta P_T = \Delta P_F + \Delta P_M \tag{A1}$$

The term ΔP_M includes only the pressure losses due to the addition of heat to the air flow in the combustion chamber. The term ΔP_F includes the pressure losses involved in bringing the air from the compressor outlet through the basket and into the combustion zone. The pressure loss due to friction in the unobstructed combustion zone is considered negligible compared with the friction pressure losses involved in conducting the air into the combustion zone. Inasmuch as $P_B = P_4 - \Delta P_F$ and ΔP_F is no greater than $0.04P_4$ for the combustion chamber, little error is made in writing

$$\frac{\Delta P_M}{P_B} \approx \frac{\Delta P_M}{P_4}$$

and

$$\frac{\Delta P_T}{P_4} = \frac{\Delta P_F}{P_4} + \frac{\Delta P_M}{P_4} \approx \frac{\Delta P_F}{P_4} + \frac{\Delta P_M}{P_B} \tag{A2}$$

Once the values of K and A for the combustion chamber are known, the values of $\Delta P_F/P_4$ and $\Delta P_M/P_B$ for known values of the

combustion-chamber inlet parameter $W\sqrt{T_4}/P_4$ and the total-temperature ratio T_5/T_4 may be obtained from the pressure-loss chart.

Use of pressure-loss chart. - The pressure-loss chart is used as follows to determine the various pressure losses: The values of K and A are assumed to be known for the combustion chamber. For known values of $W\sqrt{T_4}/P_4$ and the temperature ratio T_5/T_4, the pressure losses due to friction and momentum are then evaluated in four steps around the chart (fig. 5). The point on the ordinate of quadrant IV having the value $W\sqrt{T_4}/P_4$ is the starting point on the chart. From the curve that has the appropriate value of A, the value of M_4 is determined on the abscissa of quadrant IV and the corresponding value of $\Delta P_F/P_4$ is obtained by means of the curve in quadrant I that has the value of KA^2 for the combustion chamber. From this value of $\Delta P_F/P_4$ and the curve in quadrant II having the value of M_4 previously obtained, the value of M_B is determined on the abscissa of quadrant II. From the proper T_5/T_4 curve in quadrant III, $\Delta P_M/P_B$ is obtained on the ordinate of quadrant III. The value of $\Delta P_T/P_4$ is the sum of $\Delta P_F/P_4$ and $\Delta P_M/P_B$ according to equation (A2).

Determination of K and A. - The values of K and A for a given combustion chamber can be determined by means of the pressure-loss chart if $\Delta P_T/P_4$ and $\Delta P_F/P_4$ are known from experiment for the same value of $W\sqrt{T_4}/P_4$. The friction pressure loss ΔP_F is measured across the entire combustion chamber with air flowing through the combustion chamber without combustion taking place. In figure 20(a) the values of A and KA^2 for the type B combustion chamber were obtained from the pressure-loss chart with the following experimentally determined data:

$$\frac{\Delta P_T}{P_4} = 0.0420$$

$$\frac{\Delta P_F}{P_4} = 0.0280 \text{ (from engine windmilling data)}$$

$$\frac{\Delta P_M}{P_B} = \left(\frac{\Delta P_T}{P_4} - \frac{\Delta P_F}{P_4}\right) = 0.014 \text{ (according to equation (A2))}$$

654

$$\frac{T_5}{T_4} = 1.78$$

$$\frac{W\sqrt{T_4}}{P_4} = 0.0346$$

In the chart of figure 20(a) the following construction was used: Line B-A, quadrant III, was drawn parallel to the abscissa through the known value of $\Delta P_M/P_B$ and ended on the proper T_5/T_4 curve. Line C-D was drawn parallel to the abscissa through the value of $\Delta P_F/P_4$. Line E-F was drawn parallel to the abscissa through the value of $W\sqrt{T_4}/P_4$. Line A-G was drawn parallel to the ordinate. The intersection of lines A-G and C-D determined a value of M_4. The line H-J was drawn parallel to the ordinate through M_4 on the abscissa of quadrant I. The intersection of line H-J with line C-D determined the value of $KA^2 = 0.0269$ for the type B combustion chamber. The intersection of lines E-F and H-J similarly determined the value of A in quadrant IV equal to 0.25 square foot.

If ΔP_F is known for a different value of $W\sqrt{T_4}/P_4$ than corresponds to the known value of ΔP_T, the required value of ΔP_F corresponding to ΔP_T can be obtained from an evaluation of K in equation (1) with the known value of ΔP_F and the corresponding value $W\sqrt{T_4}/P_4$. The required value of ΔP_F is then obtained from K and the value of $W\sqrt{T_4}/P_4$ corresponding to ΔP_T.

A method of finding KA^2 and A for a combustion chamber when only the over-all loss in total pressure ΔP_T can be obtained is shown in figure 20(b). It is assumed that for a known value of $W\sqrt{T_4}/P_4$ two values of $\Delta P_T/P_4$ can be measured that correspond to two known different values of the combustion-chamber temperature ratio T_5/T_4. For both cases $\Delta P_F/P_4$ has the same value because $W\sqrt{T_4}/P_4$ is the same (equation (1)). The difference in the measured values of $\Delta P_T/P_4$ represents the difference in the values of $\Delta P_M/P_B$ (equation (A2)). This difference is set on a pair of dividers according to the scale of the ordinate of quadrant III (fig. 20(b)). With the line joining the divider points held parallel to the ordinate, one leg of the dividers is moved along one of the curves in quadrant III having one of the values of T_5/T_4 used in the investigation until the second leg of the dividers

intercepts the curve having the other value of T_5/T_4. The values of $\Delta P_M/P_B$ are thus determined for both engine conditions and the value of $\Delta P_F/P_4$ is obtained by subtracting $\Delta P_M/P_B$ from the corresponding value of $\Delta P_T/P_4$ (equation (A2)). A construction similar to that previously described for figure 20(a) can then be made to obtain A and KA^2 as shown in figure 20(b) for the experimental data given in the figure.

654

APPENDIX B

EFFECT OF PRESSURE LOSSES THROUGH COMBUSTION CHAMBER ON CYCLE EFFICIENCY

Cycle efficiency η is defined as

$$\eta = \frac{c_{p,b}\,(T_5 - T_4) - c_{p,j}\,(t_9 - t_0)}{c_{p,b}\,(T_5 - T_4)} \tag{B1}$$

The efficiency for the case with no combustion-chamber pressure losses is compared with that for which pressure losses occur in obtaining the effect of combustion-chamber pressure losses on cycle efficiency. The same engine entrance conditions, engine speed, turbine efficiency, turbine temperature ratio T_6/T_5, and temperature rise through the combustion chamber are assumed for both cases. The flow processes in the tail pipe and the tail-pipe nozzle are considered to be 100-percent efficient. The expression for the loss in cycle efficiency $\Delta\eta$ due to combustion-chamber pressure losses is

$$\begin{aligned}\Delta\eta &= \eta' - \eta \\ &= \frac{c_{p,b}\,(T_5 - T_4) - c_{p,j}\,(t_9' - t_0)}{c_{p,b}\,(T_5 - T_4)} - \frac{c_{p,b}\,(T_5 - T_4) - c_{p,j}\,(t_9' - t_0)}{c_{p,b}\,(T_5 - T_4)} \\ &= \frac{c_{p,j}\,(t_9 - t_9')}{c_{p,b}\,(T_5 - T_4)}\end{aligned} \tag{B2}$$

where η' is the cycle efficiency with no combustion-chamber pressure loss and t_9' is the temperature of the exhaust gases with no combustion-chamber pressure loss. The unprimed terms correspond to the case in which combustion-chamber pressure losses occur.

In order to use equation (B2), a relation $t_9' = f\,(T_0, P_5, P_5')$, where P_5' is the total pressure at the turbine inlet with no combustion-chamber pressure losses, must be obtained. This relation is derived in the following steps.

Turbine efficiency is given by

$$\eta_t = \frac{T_5 - T_6}{T_5\left[\left(1 - \frac{P_6}{P_5}\right)^{\frac{\gamma-1}{\gamma}}\right]}$$

from which

$$\left(\frac{P_6}{P_5}\right)^{\frac{\gamma-1}{\gamma}} = \frac{(\eta_t - 1) + \frac{T_6}{T_5}}{\eta_t} = \left(\frac{P_6'}{P_5'}\right)^{\frac{\gamma-1}{\gamma}} \tag{B3}$$

as T_6/T_5 is assumed equal to T_6'/T_5' and η_t is assumed to be the same for the cases with and without combustion-chamber pressure losses.

The isentropic adiabatic relation and the equation of state for a perfect gas give

$$\frac{P^{\frac{1}{\gamma}}}{\rho_T} = \frac{p^{\frac{1}{\gamma}}}{\rho} = C^{\frac{1}{\gamma}} = \left(\frac{P}{\rho_T}\right) P^{\frac{1-\gamma}{\gamma}} = RTP^{\frac{1-\gamma}{\gamma}} = RT\left(\frac{1}{P}\right)^{\frac{\gamma-1}{\gamma}} = Rt\left(\frac{1}{p}\right)^{\frac{\gamma-1}{\gamma}}$$

At the turbine inlet, then

$$\left(\frac{C_5}{C_5'}\right)^{\frac{1}{\gamma}} = \frac{RT_5}{RT_5'}\left(\frac{P_5'}{P_5}\right)^{\frac{\gamma-1}{\gamma}}$$

and inasmuch as $T_5 = T_5'$

$$\left(\frac{C_5}{C_5'}\right)^{\frac{1}{\gamma}} = \left(\frac{P_5'}{P_5}\right)^{\frac{\gamma-1}{\gamma}} \tag{B4}$$

Likewise, because $T_6 = T_6'$

$$\left(\frac{C_6}{C_6'}\right)^{\frac{1}{\gamma}} = \left(\frac{P_6'}{P_6}\right)^{\frac{\gamma-1}{\gamma}}$$

and

$$\left(\frac{C_5}{C_5'}\frac{C_6'}{C_6}\right)^{\frac{1}{\gamma}} = \left(\frac{P_5'}{P_6'}\frac{P_6}{P_5}\right)^{\frac{\gamma-1}{\gamma}}$$

From equation (B3)

$$\left(\frac{P_5'}{P_6'}\frac{P_6}{P_5}\right)^{\frac{\gamma-1}{\gamma}} = 1$$

therefore

$$\frac{C_5}{C_5'} = \frac{C_6}{C_6'}$$

From equation (B4) and from the assumption that the flow is adiabatic and isentropic between stations 6 and 9 $(C_6 = C_9)$

$$\left(\frac{P_5}{P_5'}\right)^{\frac{\gamma-1}{\gamma}} = \left(\frac{C_5'}{C_5}\right)^{\frac{1}{\gamma}} = \left(\frac{C_6'}{C_6}\right)^{\frac{1}{\gamma}} = \frac{t_9'}{t_9}\left(\frac{p_9}{p_9'}\right)^{\frac{\gamma-1}{\gamma}}$$

Inasmuch as $p_9 = p_0 = p_9'$, where p_0 is the free-stream static pressure

$$\left(\frac{P_5}{P_5'}\right)^{\frac{\gamma-1}{\gamma}} = \frac{t_9'}{t_9}$$

where γ is the average value between stations 5 and 9.

Because it represents the total pressure at the combustion-chamber outlet for the case of no pressure losses, $P_5' = P_4$; thus

$$\left(\frac{P_5}{P_4}\right)^{\frac{\gamma-1}{\gamma}} = \frac{t_9'}{t_9} \tag{B5}$$

By substitution of equation (B5) in equation (B2)

$$\Delta\eta = \frac{c_{p,j}t_9 \left[1 - \left(\frac{P_5}{P_4}\right)^{\frac{\gamma-1}{\gamma}}\right]}{c_{p,b}\,(T_5 - T_4)} \tag{B6}$$

where

$$\frac{P_5}{P_4} = \frac{P_4 - \Delta P_T}{P_4} = 1 - \frac{\Delta P_T}{P_4}$$

The assumption that the engine speed, the temperature rise across the combustion chamber, and the total-temperature ratio across the turbine are the same for the cases with and without pressure losses across the combustion chamber represents an approximation. In order to maintain the engine speed with the reduced pressure drop across the turbine resulting from the combustion-chamber pressure losses, higher turbine-inlet temperatures would be required than for the case without pressure losses.

REFERENCES

1. Fleming, William A.: Altitude-Wind-Tunnel Investigation of a 4000-Pound-Thrust Axial-Flow Turbojet Engine. I - Performance and Windmilling Characteristics. NACA RM No. E8F09, 1948.

2. Fleming, William A.: Altitude-Wind-Tunnel Investigation of a 4000-Pound-Thrust Axial-Flow Turbojet Engine. II - Operational Characteristics. NACA RM No. E8F09a, 1948.

3. Fleming, William A., and Golladay, Richard L.: Altitude-Wind-Tunnel Investigation of a 4000-Pound-Thrust Axial-Flow Turbojet Engine. III - Performance Characteristics with the High-Flow Compressor. NACA RM No. E8F09b, 1948.

4. Dietz, Robert O., Jr., and Suozzi, Frank L.: Altitude-Wind-Tunnel Investigation of a 4000-Pound-Thrust Axial-Flow Turbojet Engine. IV - Analysis of Compressor Performance. NACA RM No. E8F09c, 1948.

5. Krebs, Richard P., and Hensley, Reece V.: Altitude-Wind-Tunnel Investigation of a 4000-Pound-Thrust Axial-Flow Turbojet Engine. V - Analysis of Turbine Performance. NACA RM No. E8F09d, 1948.

6. Pinkel, I. Irving, and Shames, Harold: Analysis of Jet-Propulsion Engine Combustion-Chamber Pressure Losses. NACA TN No. 1180, 1947.

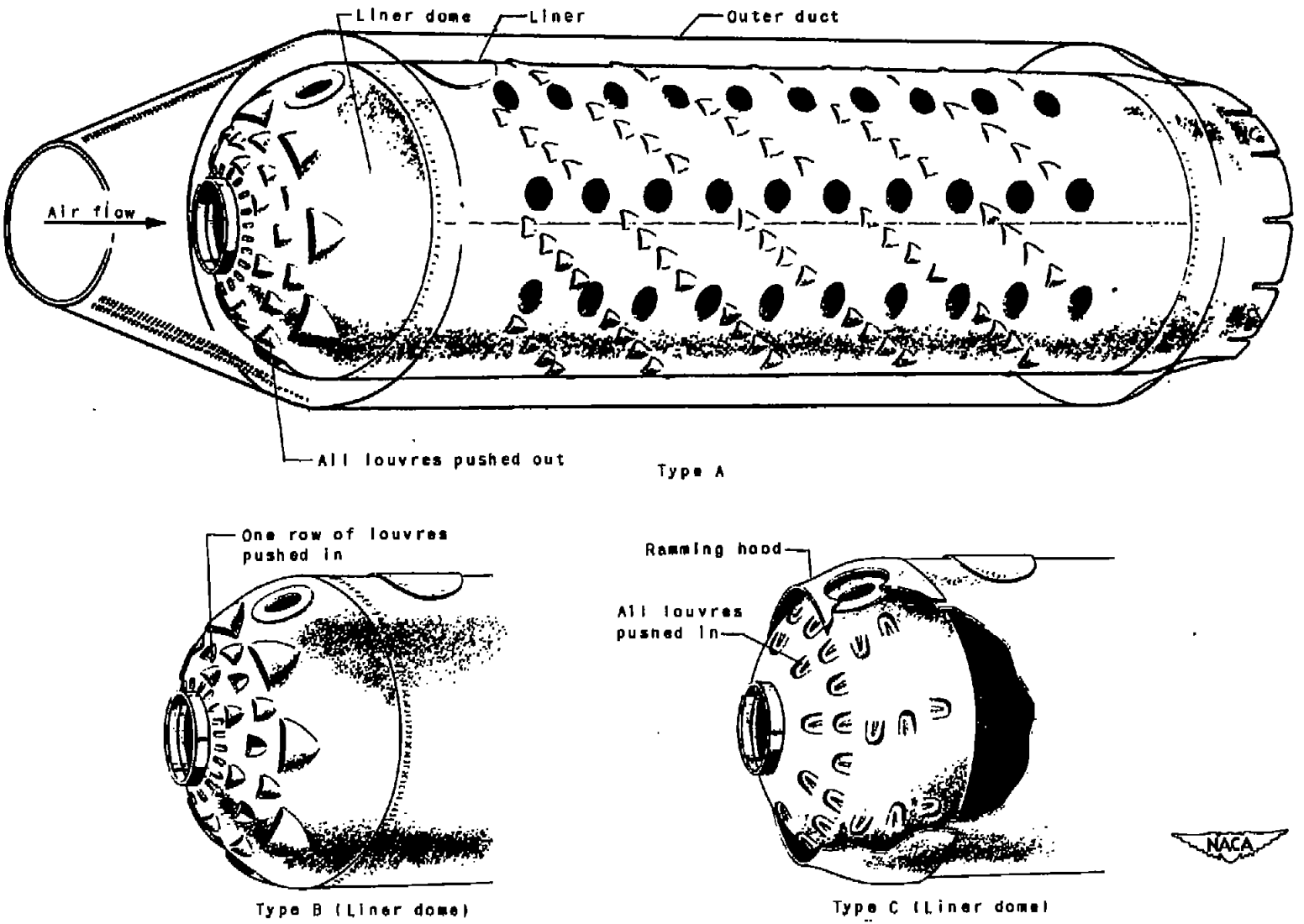

Figure 1. - Types A, B, and C combustion chambers used with 4000-pound-thrust axial-flow turbojet engine illustrating difference in primary-air entrance arrangement.

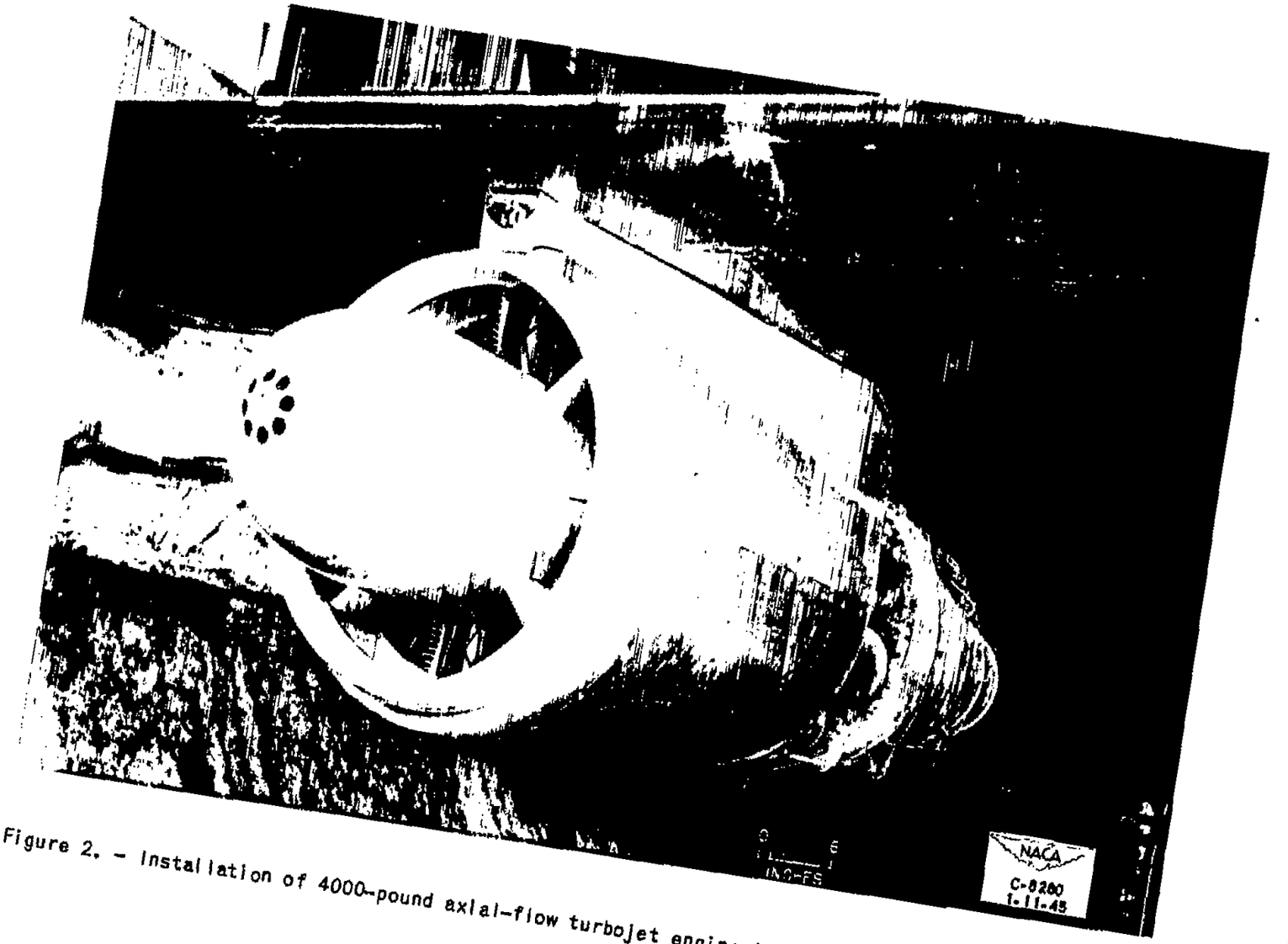

Figure 2. - Installation of 4000-pound axial-flow turbojet engine in Cleveland altitude wind tunnel.

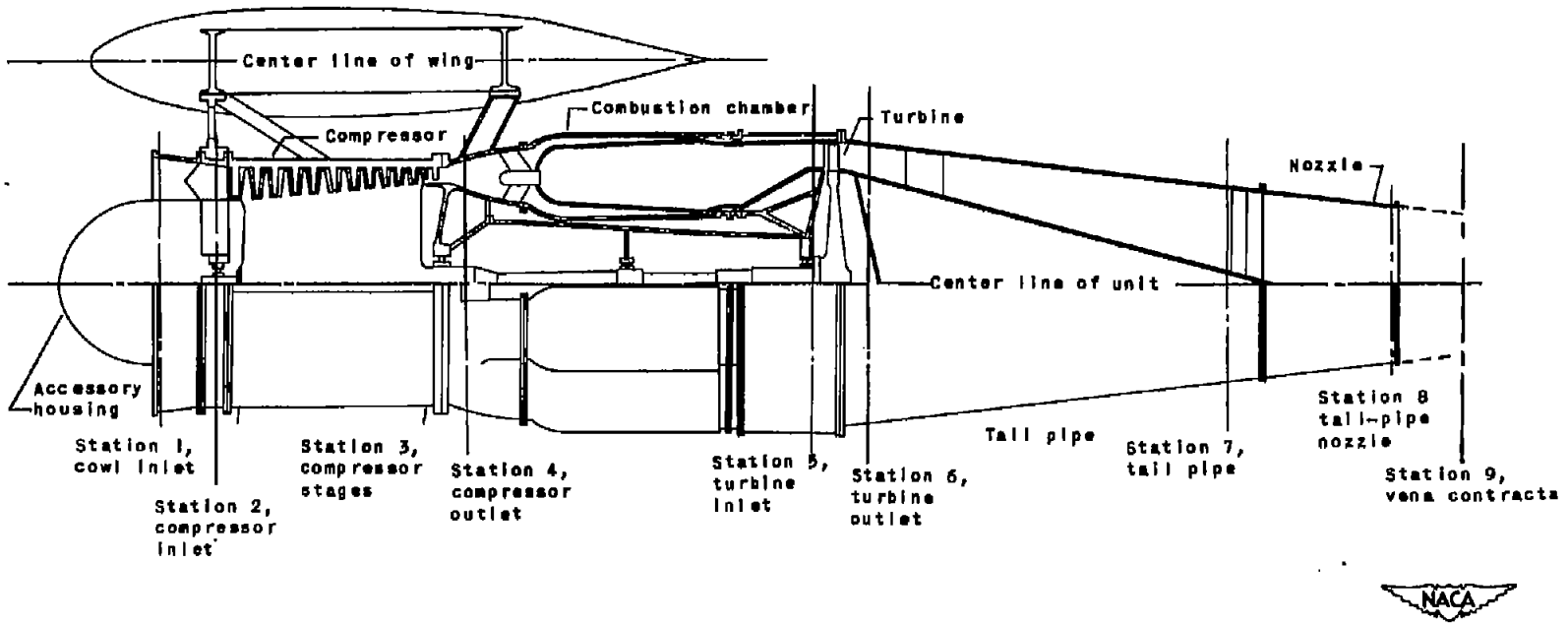

Figure 3. - Side view of 4000-pound-thrust axial-flow turbojet engine installation showing measuring stations.

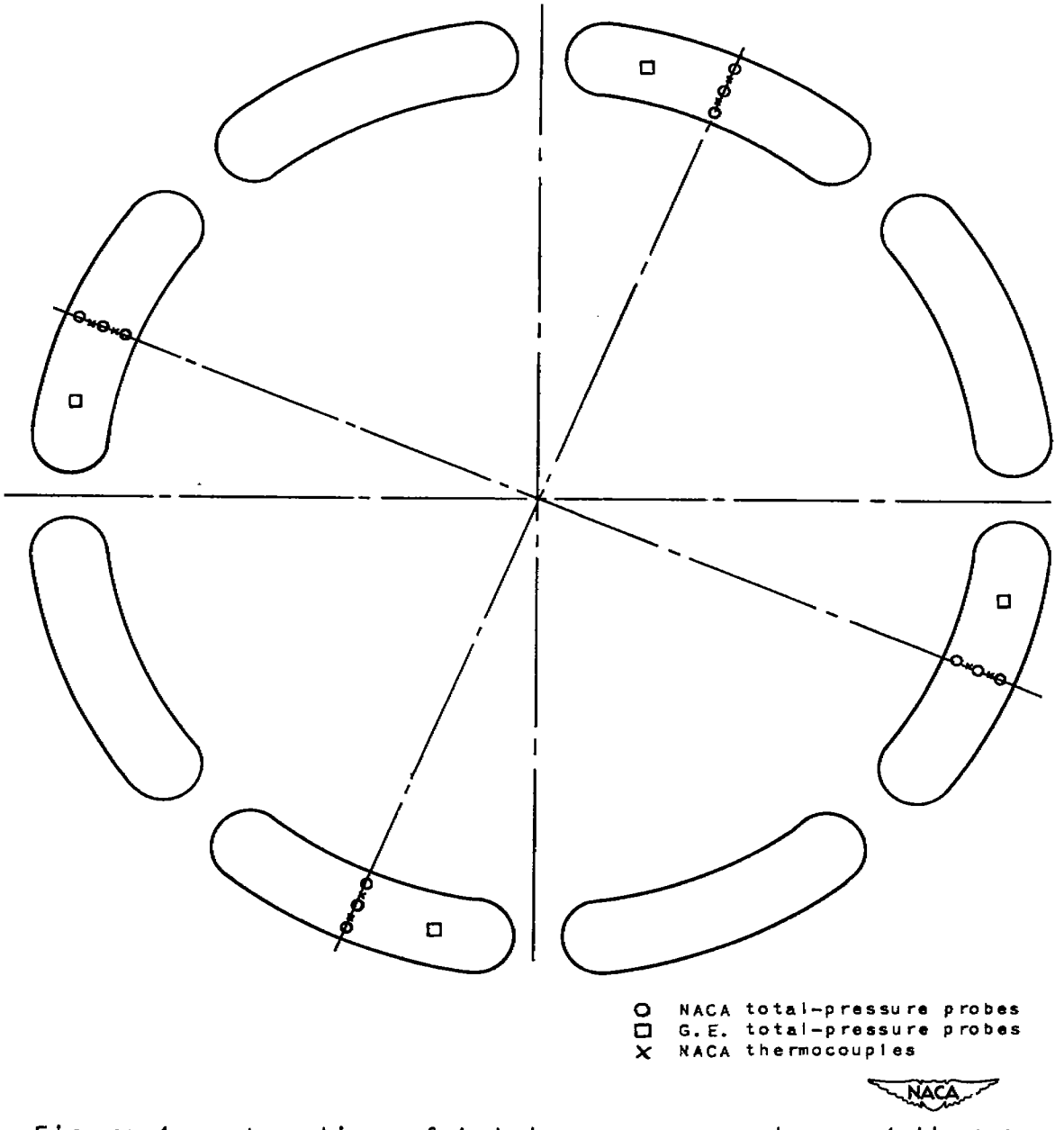

Figure 4. - Location of total-pressure probes and thermocouples at compressor outlet, station 4.

024

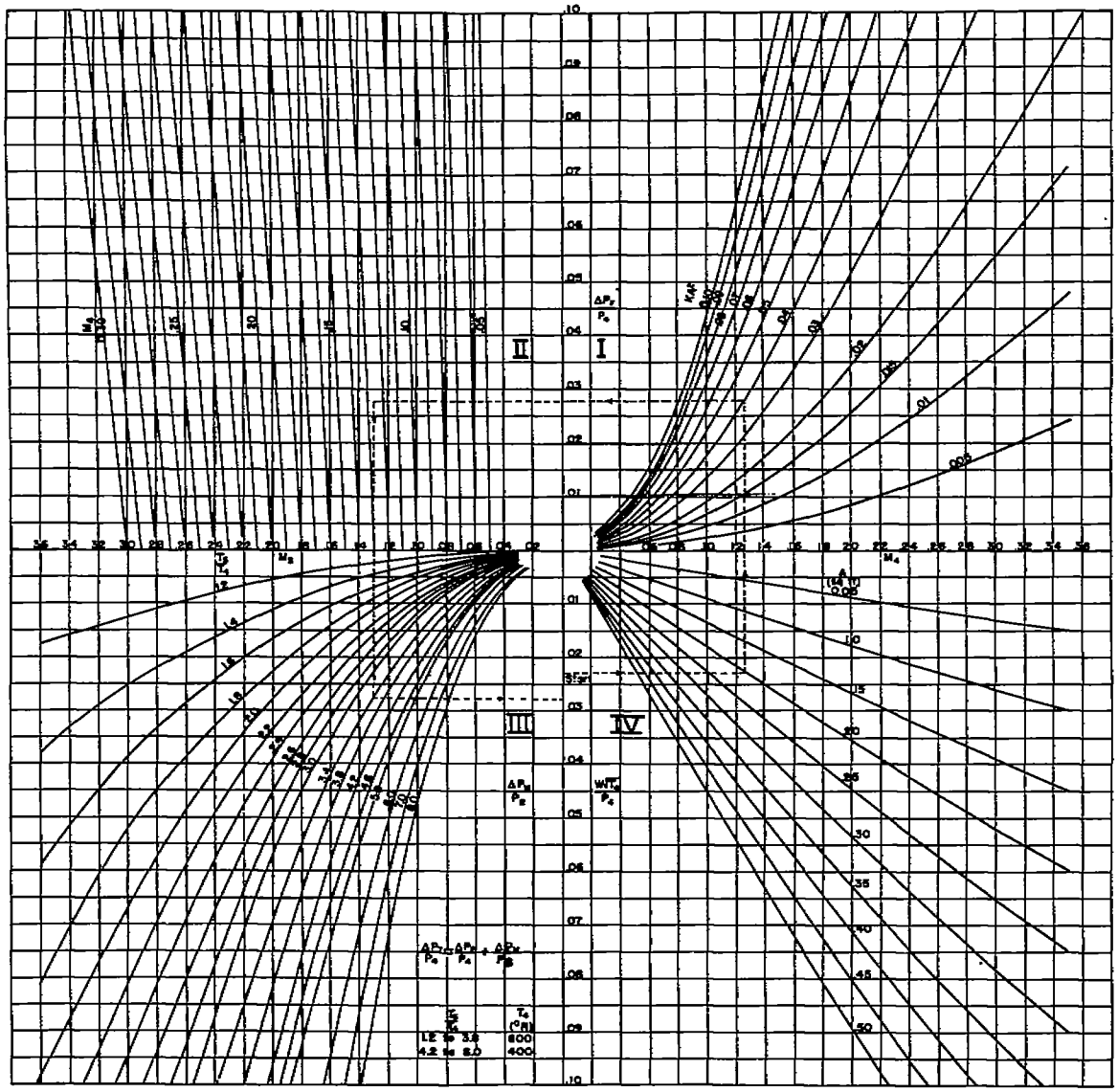

Figure 5. - Combustion-chamber pressure-loss chart. (A 17- by 22-inch copy of this chart can be obtained upon request from the NACA).

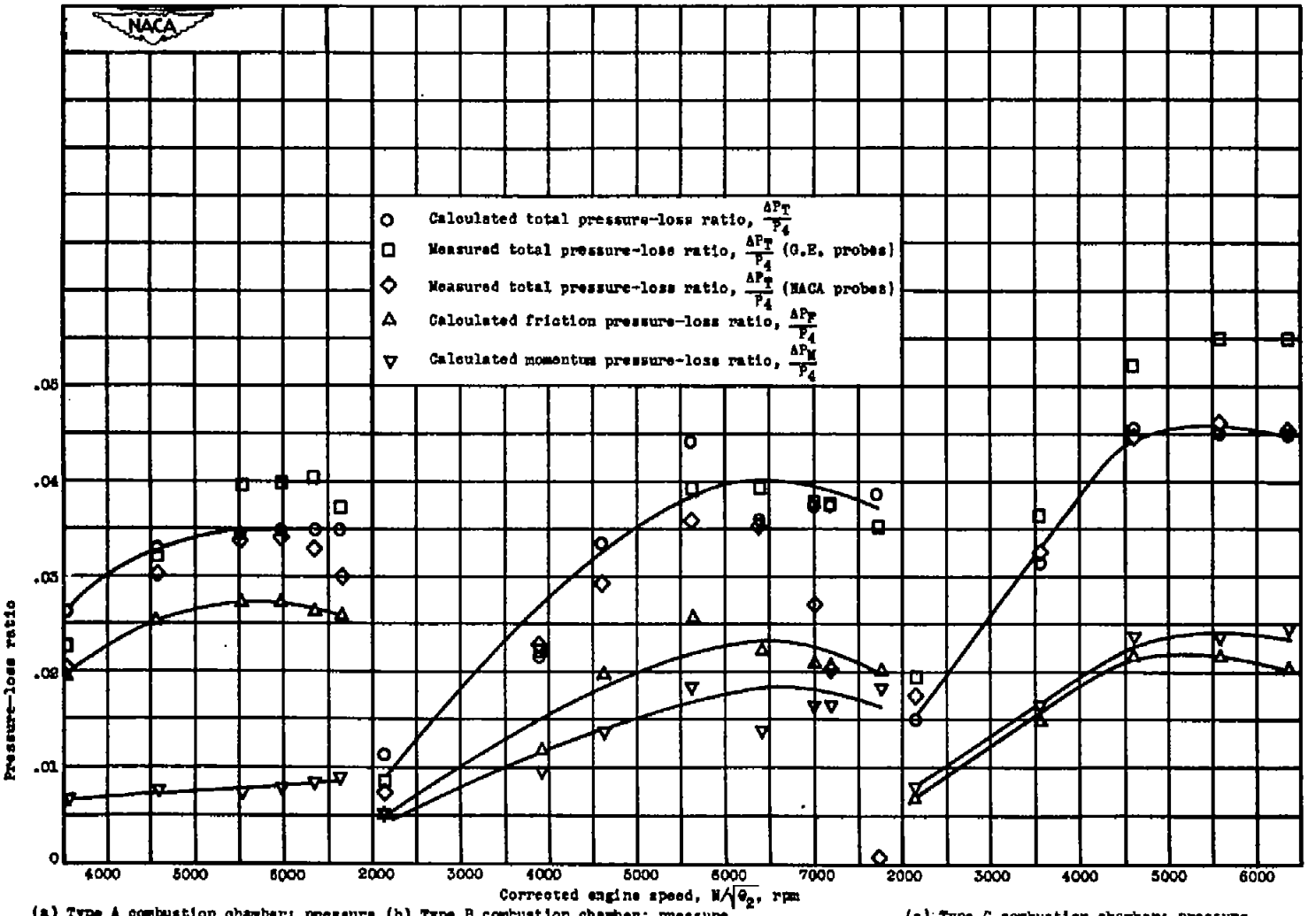

(a) Type A combustion chamber; pressure altitude, 5000 feet; low-flow compressor; small turbine nozzle; $16\frac{1}{4}$-inch-diameter tail-pipe nozzle.

(b) Type B combustion chamber; pressure altitude, 5000 feet; low-flow compressor; standard turbine nozzle; $16\frac{3}{4}$-inch-diameter tail-pipe nozzle.

(c) Type C combustion chamber; pressure altitude, 5000 feet; high-flow compressor; large turbine nozzle; 18-inch-diameter tail-pipe nozzle.

Figure 6.- Comparison of measured pressure losses with losses calculated by means of pressure chart. Static conditions.

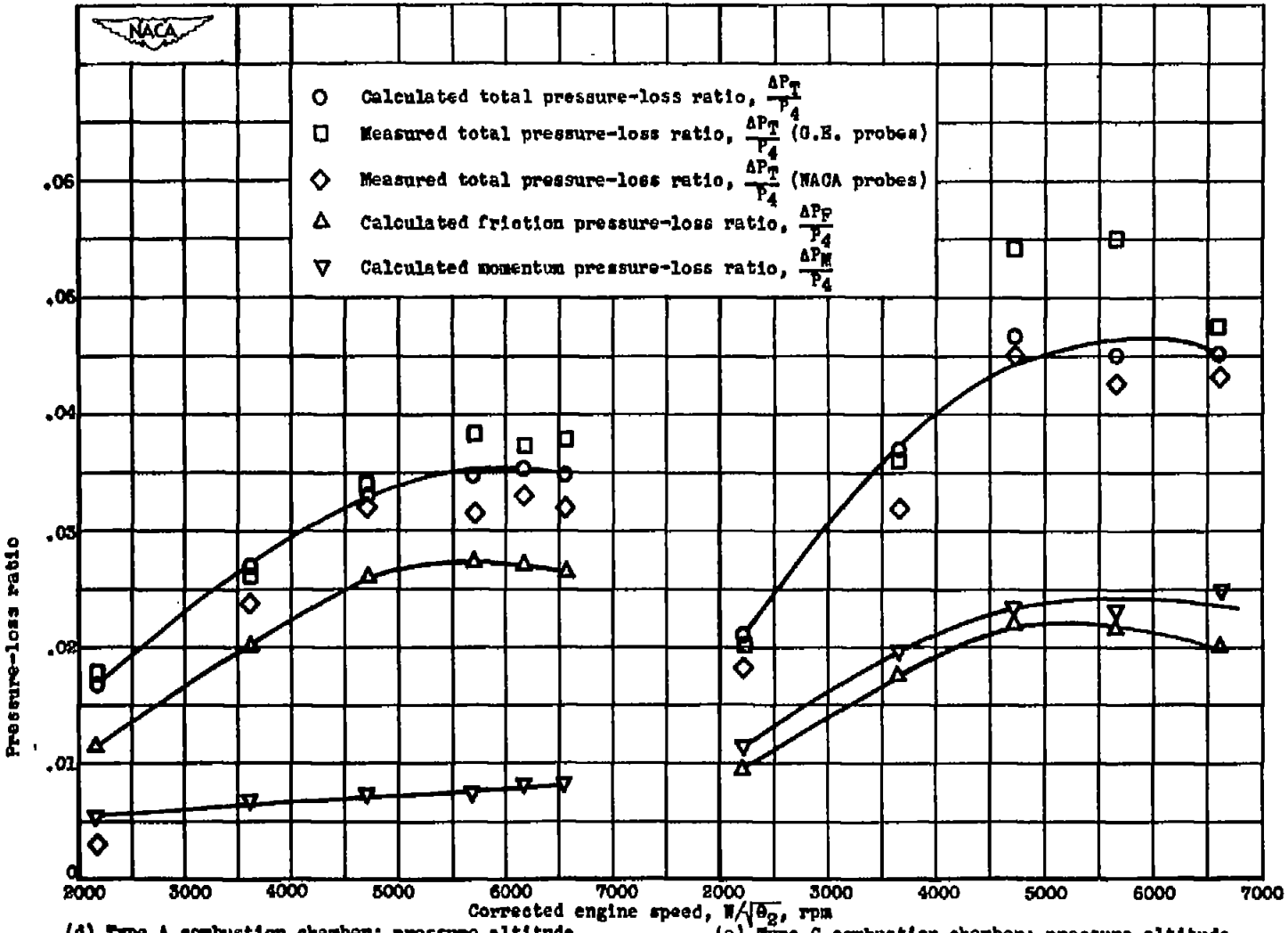

(d) Type A combustion chamber; pressure altitude, 10,000 feet; low-flow compressor; small turbine nozzle; 16¼-inch-diameter tail-pipe nozzle.

(e) Type C combustion chamber; pressure altitude, 10,000 feet; high-flow compressor; large turbine nozzle; 18-inch-diameter tail-pipe nozzle.

Figure 6.- Continued. Comparison of measured pressure losses with losses calculated by means of pressure chart. Static conditions.

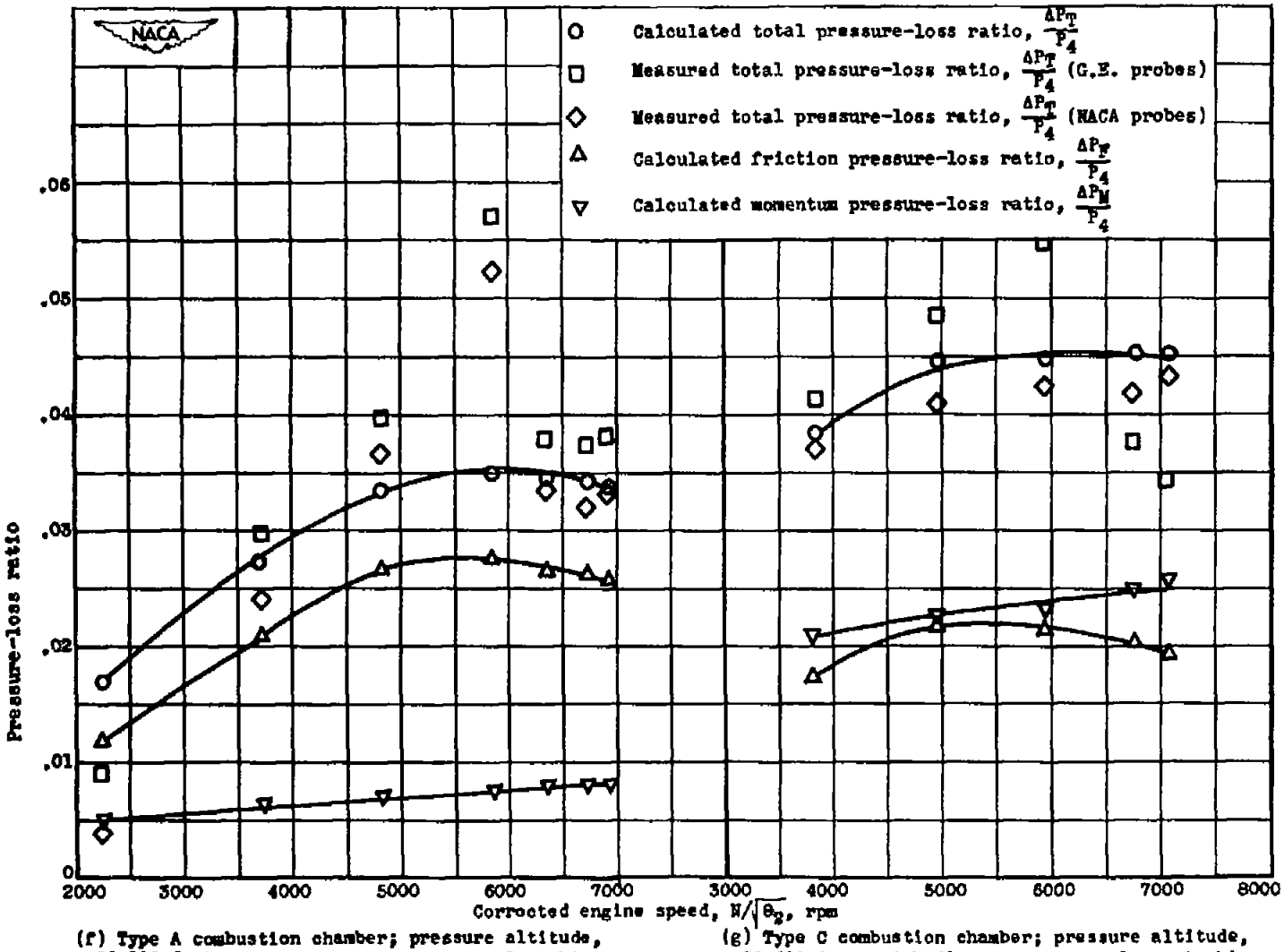

(f) Type A combustion chamber; pressure altitude, 20,000 feet; low-flow compressor; small turbine nozzle; $16\frac{1}{4}$-inch-diameter tail-pipe nozzle.

(g) Type C combustion chamber; pressure altitude, 20,000 feet; high-flow compressor; large turbine nozzle; 18-inch-diameter tail-pipe nozzle.

Figure 6.- Continued. Comparison of measured pressure losses with losses calculated by means of pressure chart. Static conditions.

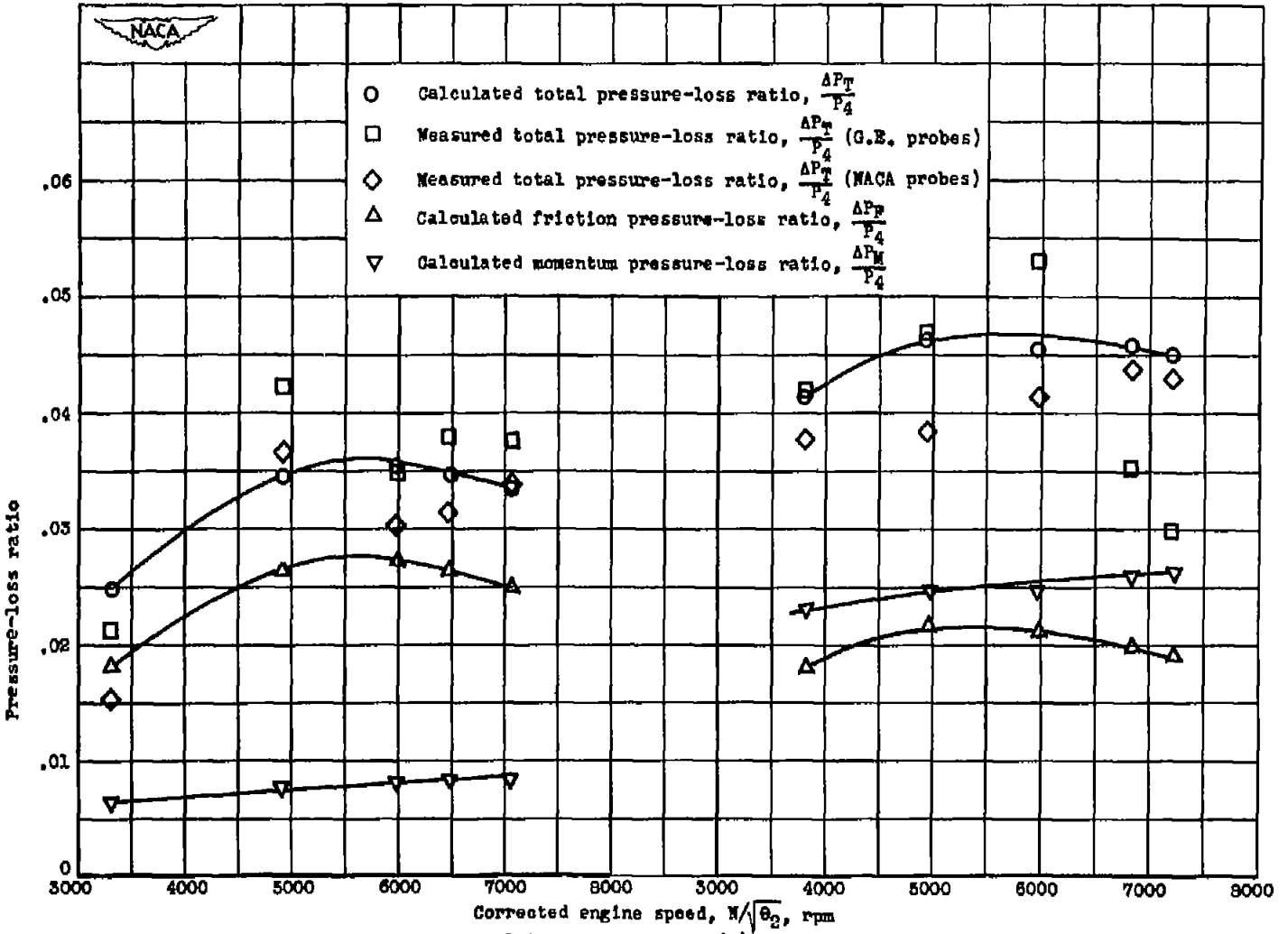

(h) Type A combustion chamber; pressure altitude, 30,000 feet; low-flow compressor; small turbine nozzle; $16\frac{1}{4}$-inch-diameter tail-pipe nozzle.

(i) Type C combustion chamber; pressure altitude, 30,000 feet; high-flow compressor; large turbine nozzle; 18-inch-diameter tail-pipe nozzle.

Figure 6.- Continued. Comparison of measured pressure losses with losses calculated by means of pressure chart. Static conditions.

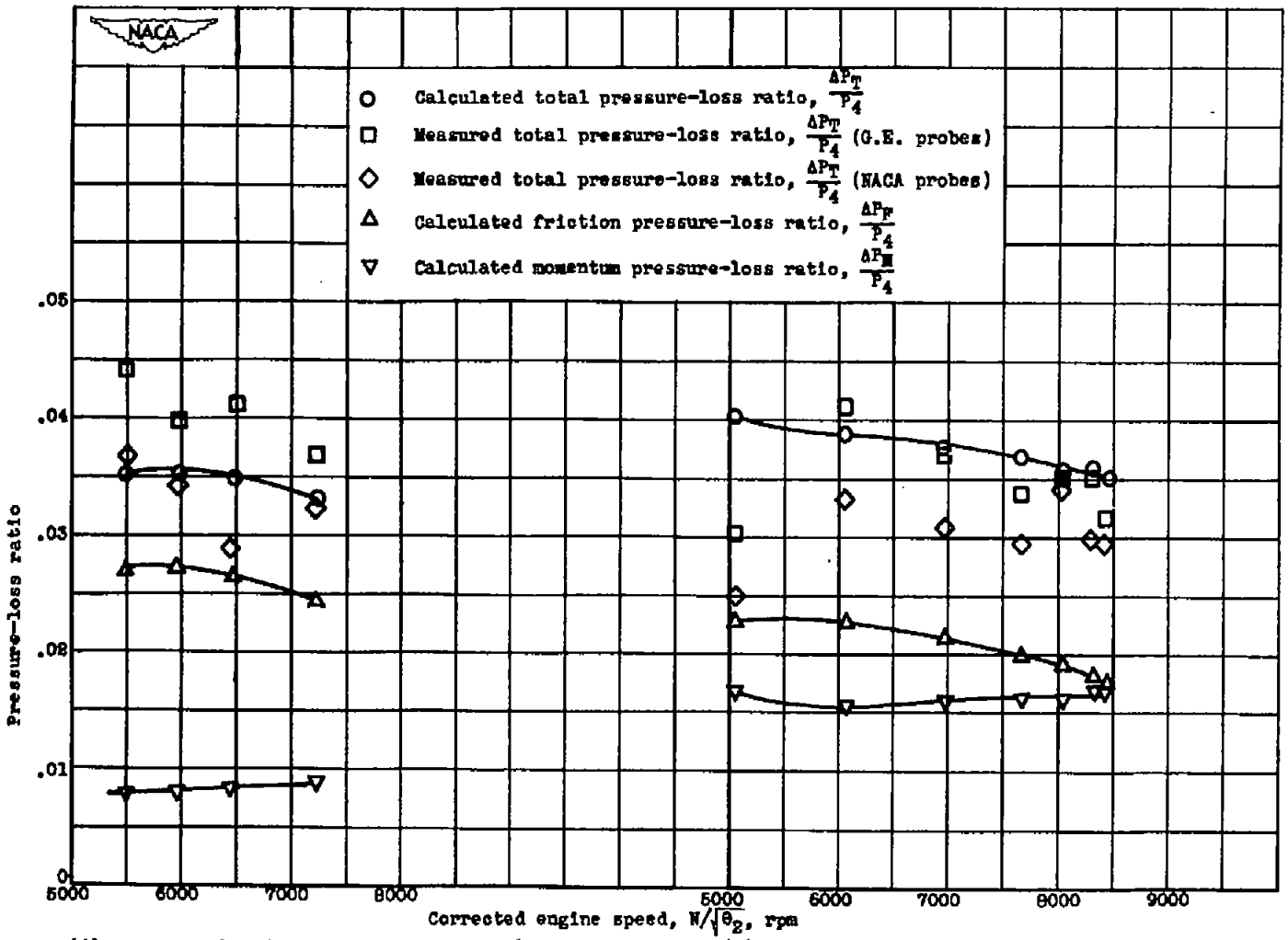

(j) Type A combustion chamber; pressure altitude, 40,000 feet; low-flow compressor; small turbine nozzle; $16\frac{1}{4}$-inch-diameter tail-pipe nozzle.

(k) Type B combustion chamber; pressure altitude, 40,000 feet; low-flow compressor; standard turbine nozzle; $16\frac{3}{4}$-inch-diameter tail-pipe nozzle.

Figure 6.- Concluded. Comparison of measured pressure losses with losses calculated by means of pressure chart. Static conditions.

654

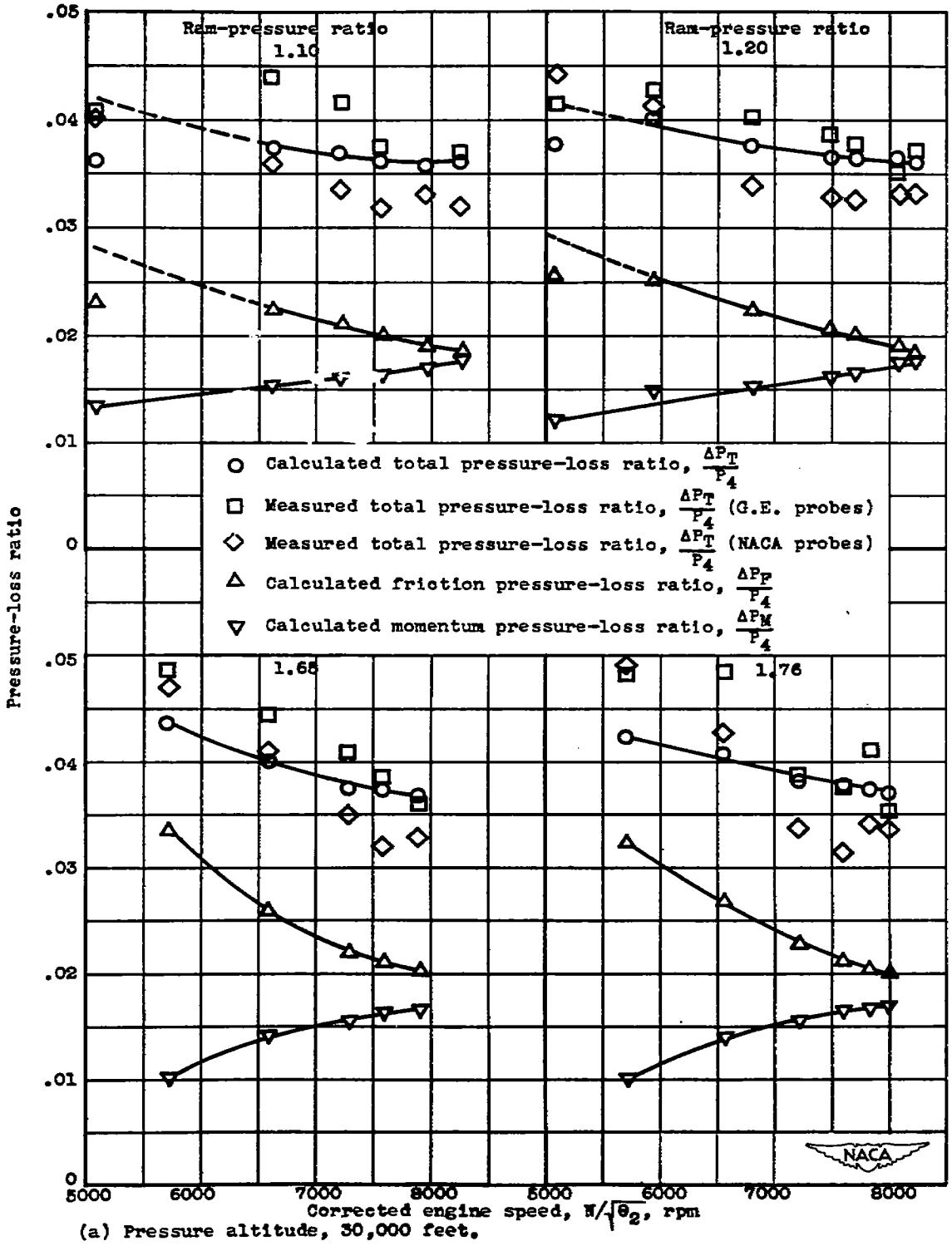

(a) Pressure altitude, 30,000 feet.

Figure 7.- Variation of pressure losses with ram pressure ratio for type B combustion chamber. Low-flow compressor; standard turbine nozzle; $16\frac{3}{4}$-inch-diameter tail-pipe nozzle.

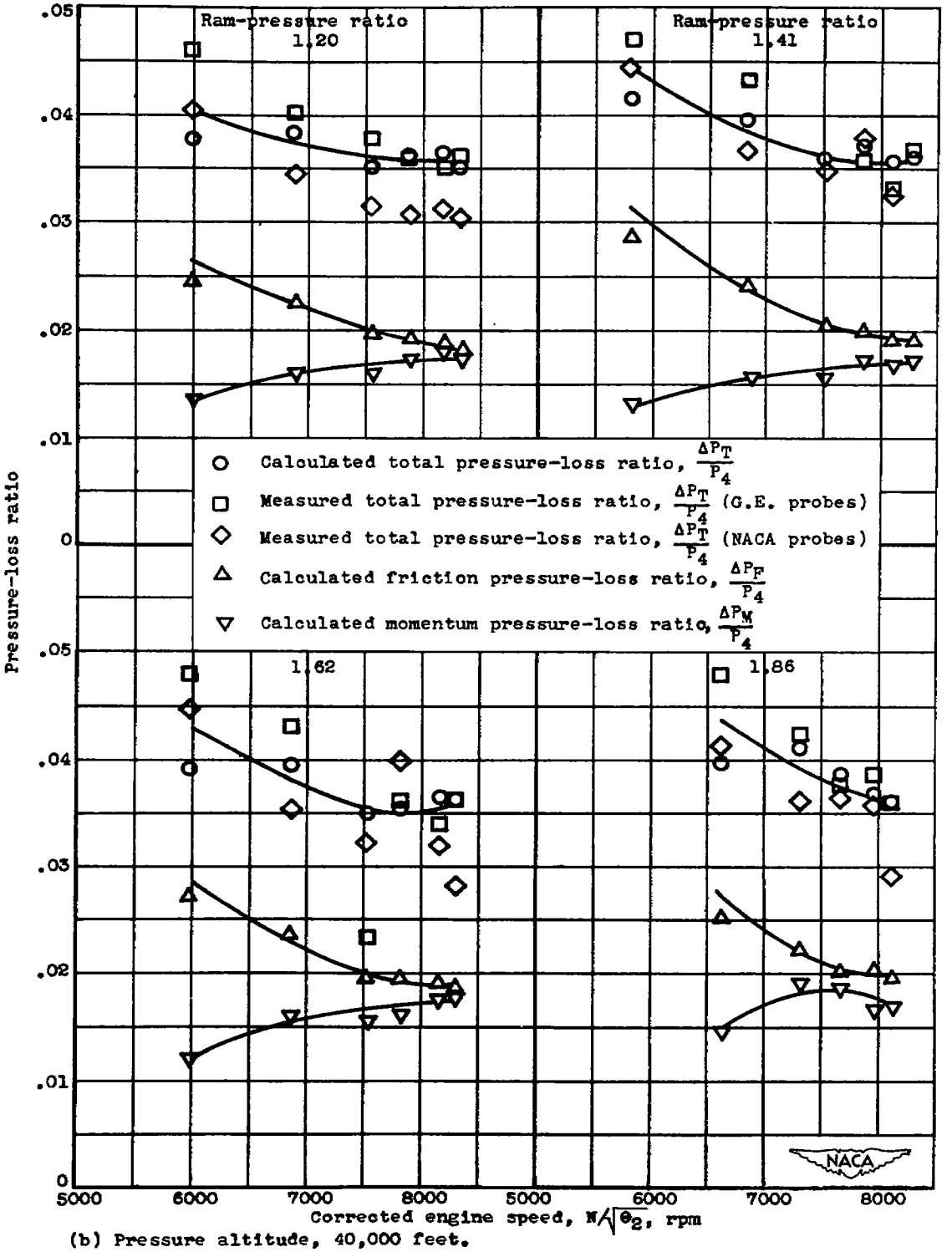

(b) Pressure altitude, 40,000 feet.

Figure 7.- Concluded. Variation of pressure losses with ram pressure ratio for type B combustion chamber. Low-flow compressor; standard turbine nozzle; $16\frac{3}{4}$-inch-diameter tail-pipe nozzle.

654

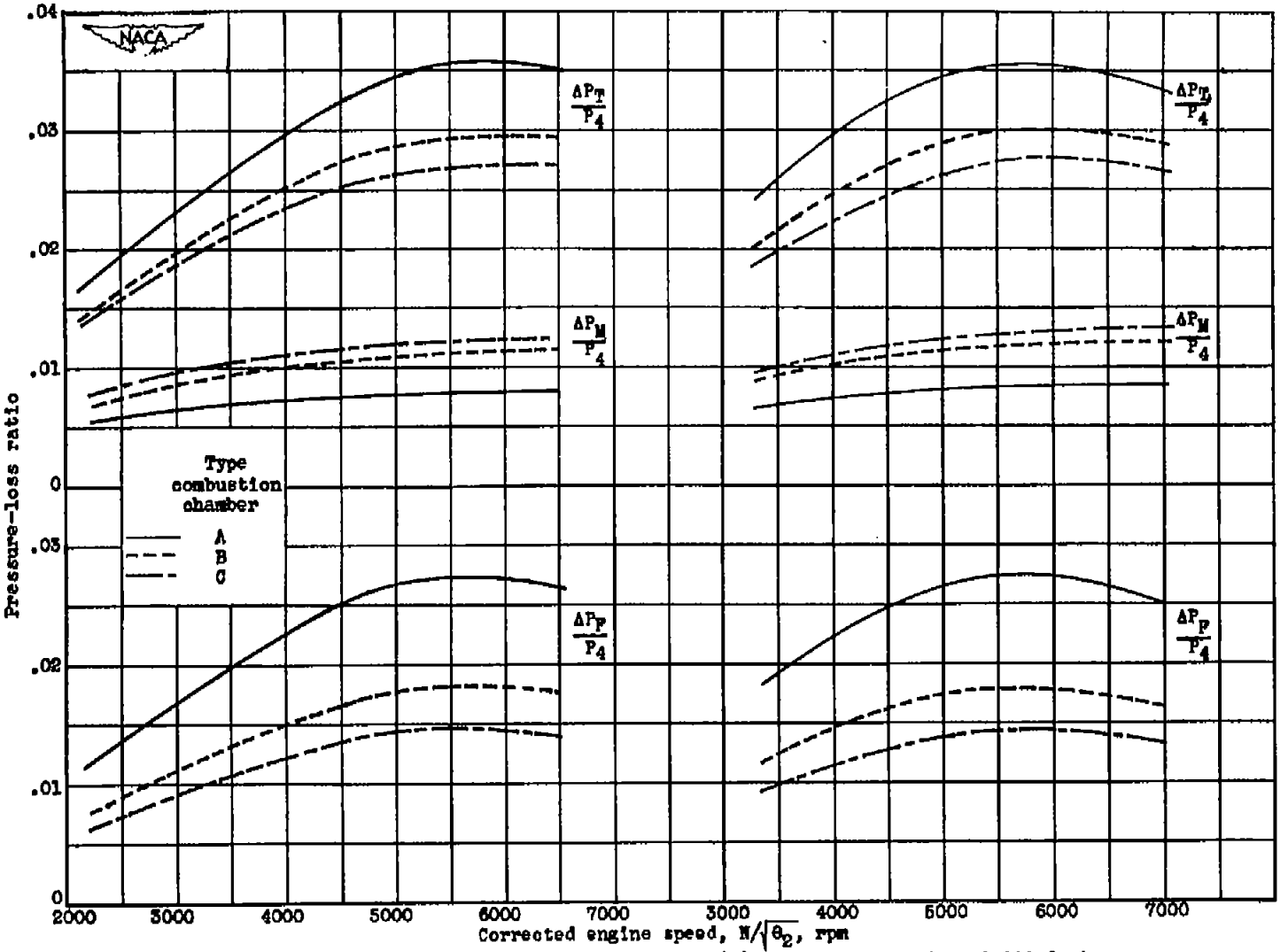

(a) Pressure altitude, 10,000 feet. (b) Pressure altitude, 30,000 feet.

Figure 8.- Comparison of calculated pressure-loss characteristics of types A, B, and C combustion chambers. Static conditions; low-flow compressor; small turbine nozzle; $16\frac{1}{4}$-inch-diameter tail-pipe nozzle.

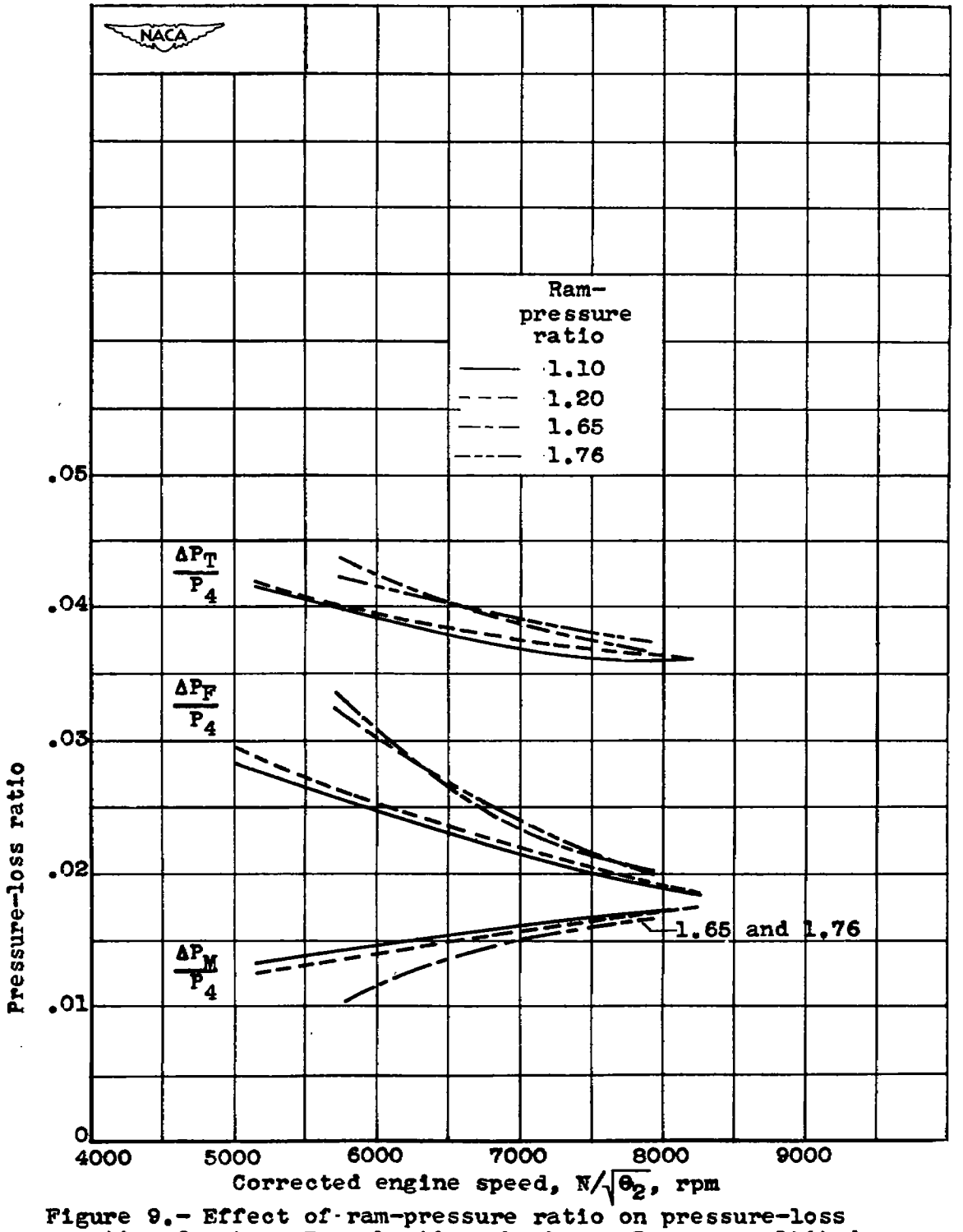

Figure 9.- Effect of ram-pressure ratio on pressure-loss ratios for type B combustion chamber. Pressure altitude, 30,000 feet; low-flow compressor; standard turbine nozzle; $16\frac{3}{4}$-inch-diameter tail-pipe nozzle.

654

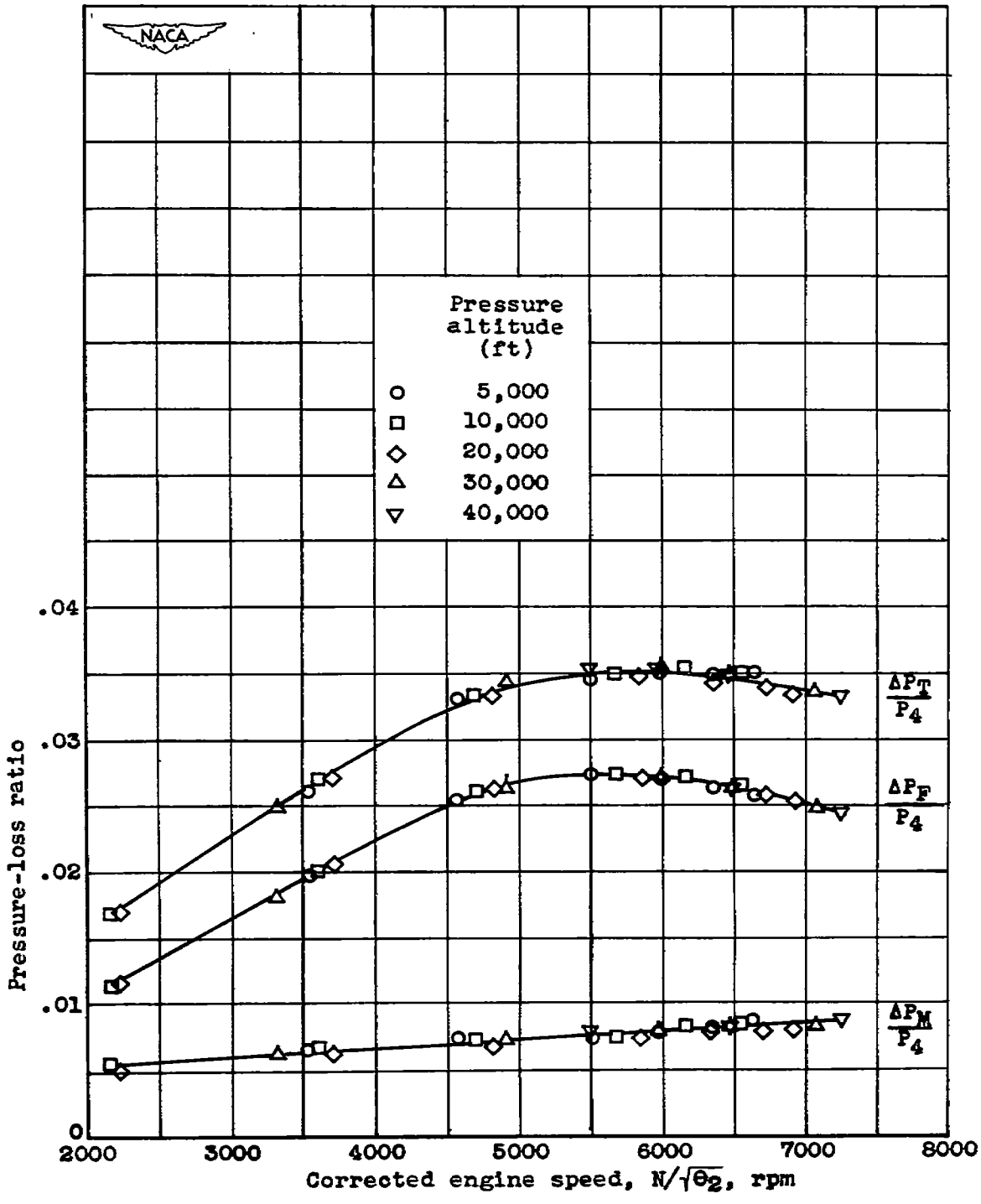

Figure 10.- Effect of pressure altitude on calculated pressure-loss ratios for type A combustion chamber. Static conditions; low-flow compressor; small turbine nozzle; $16\frac{1}{4}$-inch-diameter tail-pipe nozzle.

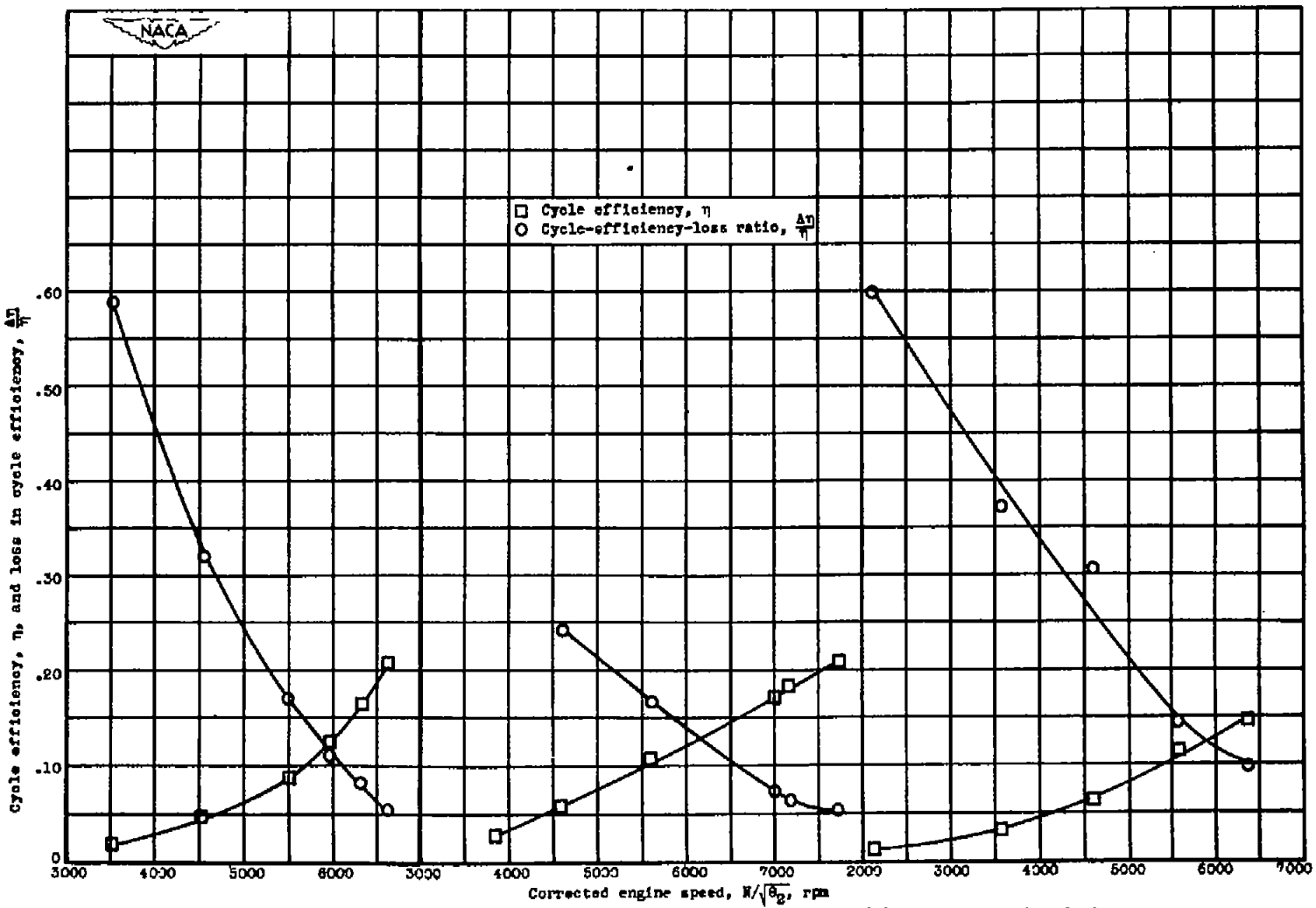

(a) Type A combustion chamber; pressure altitude, 5000 feet; low-flow compressor; small turbine nozzle; $16\frac{1}{4}$-inch-diameter tail-pipe nozzle.

(b) Type B combustion chamber; pressure altitude, 5000 feet; low-flow compressor; standard turbine nozzle; $16\frac{3}{4}$-inch-diameter tail-pipe nozzle.

(c) Type C combustion chamber; pressure altitude, 5000 feet; high-flow compressor; large turbine nozzle; 18-inch-diameter tail-pipe nozzle.

Figure 11.- Effect of altitude on loss in cycle efficiency due to combustion-chamber pressure losses. Static conditions.

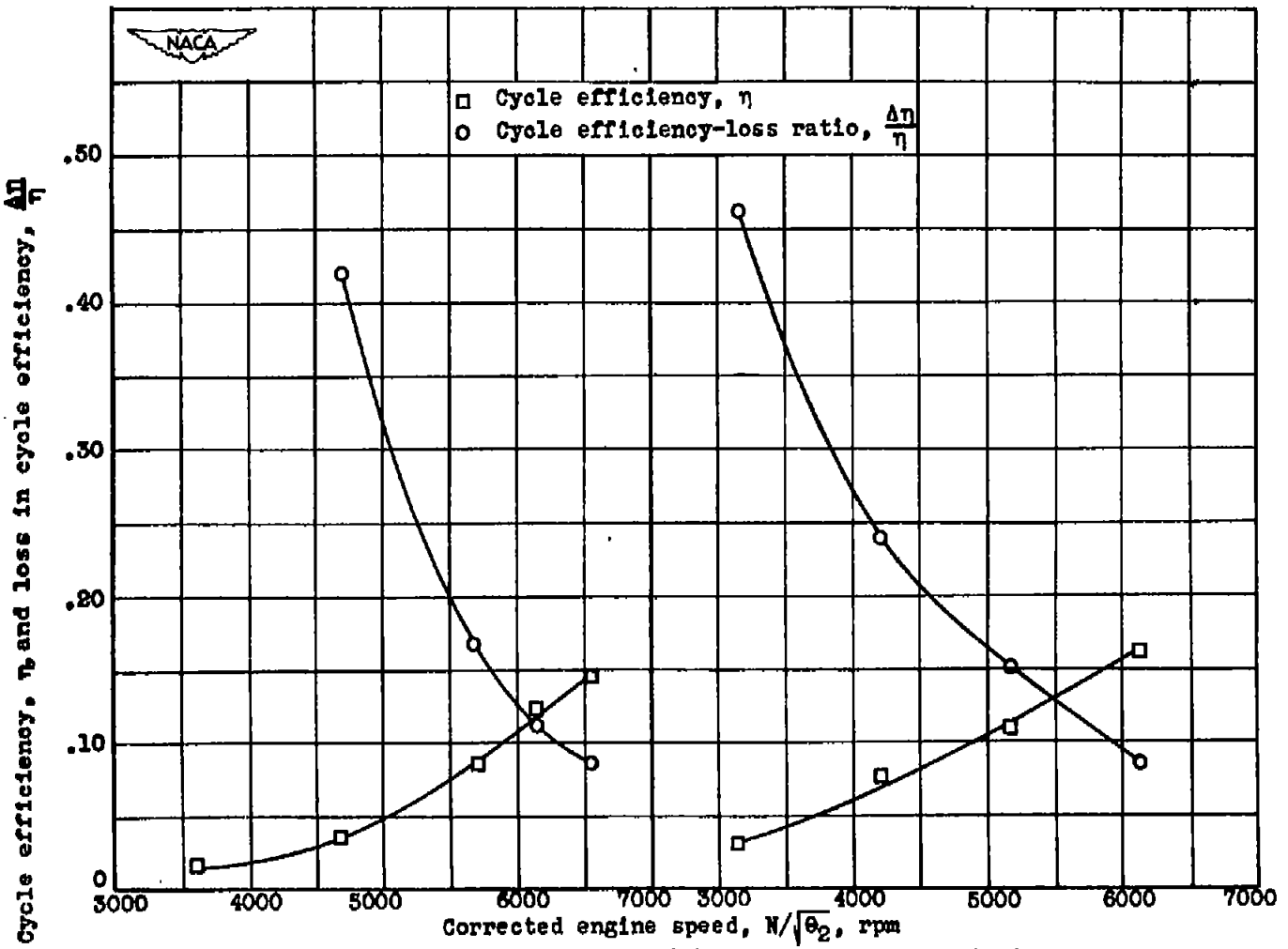

(d) Type A combustion chamber; pressure altitude, 10,000 feet; low-flow compressor; small turbine nozzle; $16\frac{1}{4}$-inch-diameter tail-pipe nozzle.

(e) Type C combustion chamber; pressure altitude, 10,000 feet; high-flow compressor; large turbine nozzle; 18-inch-diameter tail-pipe nozzle.

Figure 11.- Continued. Effect of altitude on loss in cycle efficiency due to combustion-chamber pressure losses. Static conditions.

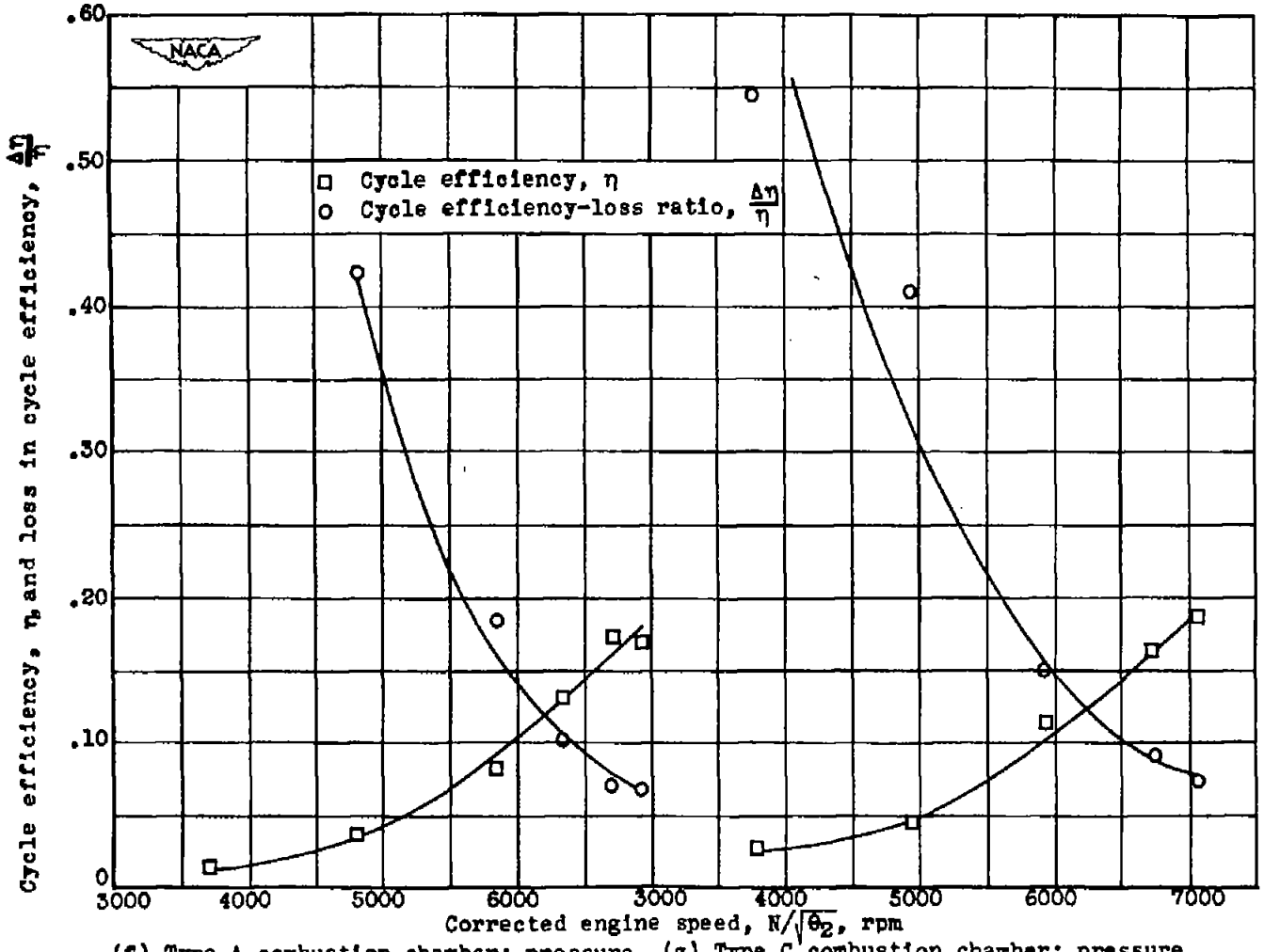

(f) Type A combustion chamber; pressure altitude, 20,000 feet; low-flow compressor; small turbine nozzle; $16\frac{1}{4}$-inch-diameter tail-pipe nozzle.

(g) Type C combustion chamber; pressure altitude, 20,000 feet; high-flow compressor; large turbine nozzle; 18-inch-diameter tail-pipe nozzle.

Figure 11.- Continued. Effect of altitude on loss in cycle efficiency due to combustion-chamber pressure losses. Static conditions.

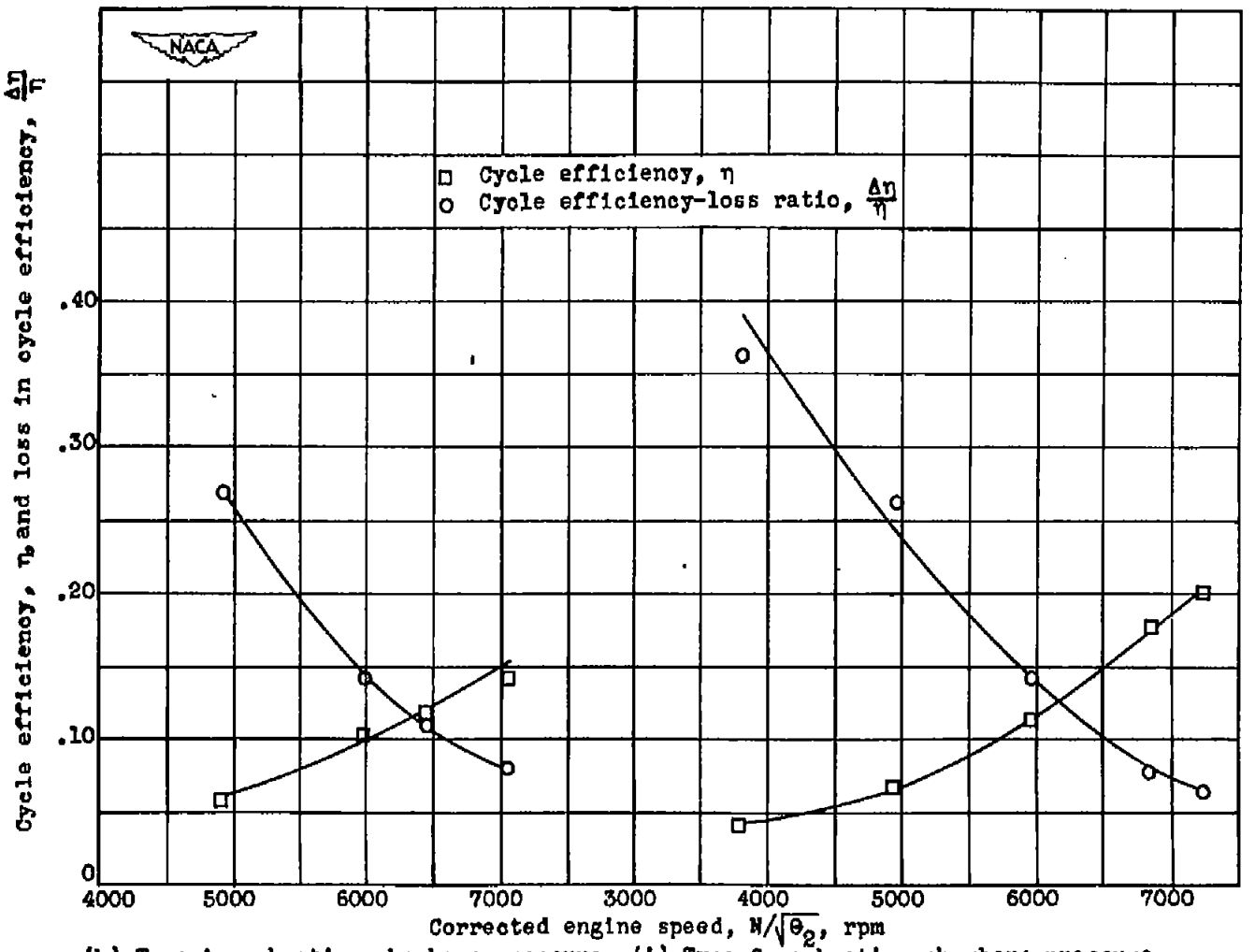

(h) Type A combustion chamber; pressure altitude, 30,000 feet; low-flow compressor; small turbine nozzle; $16\frac{1}{4}$-inch-diameter tail-pipe nozzle.

(i) Type C combustion chamber; pressure altitude, 30,000 feet; high-flow compressor; large turbine nozzle; 18-inch-diameter tail-pipe nozzle.

Figure 11.- Continued. Effect of altitude on loss in cycle efficiency due to combustion-chamber pressure losses. Static conditions.

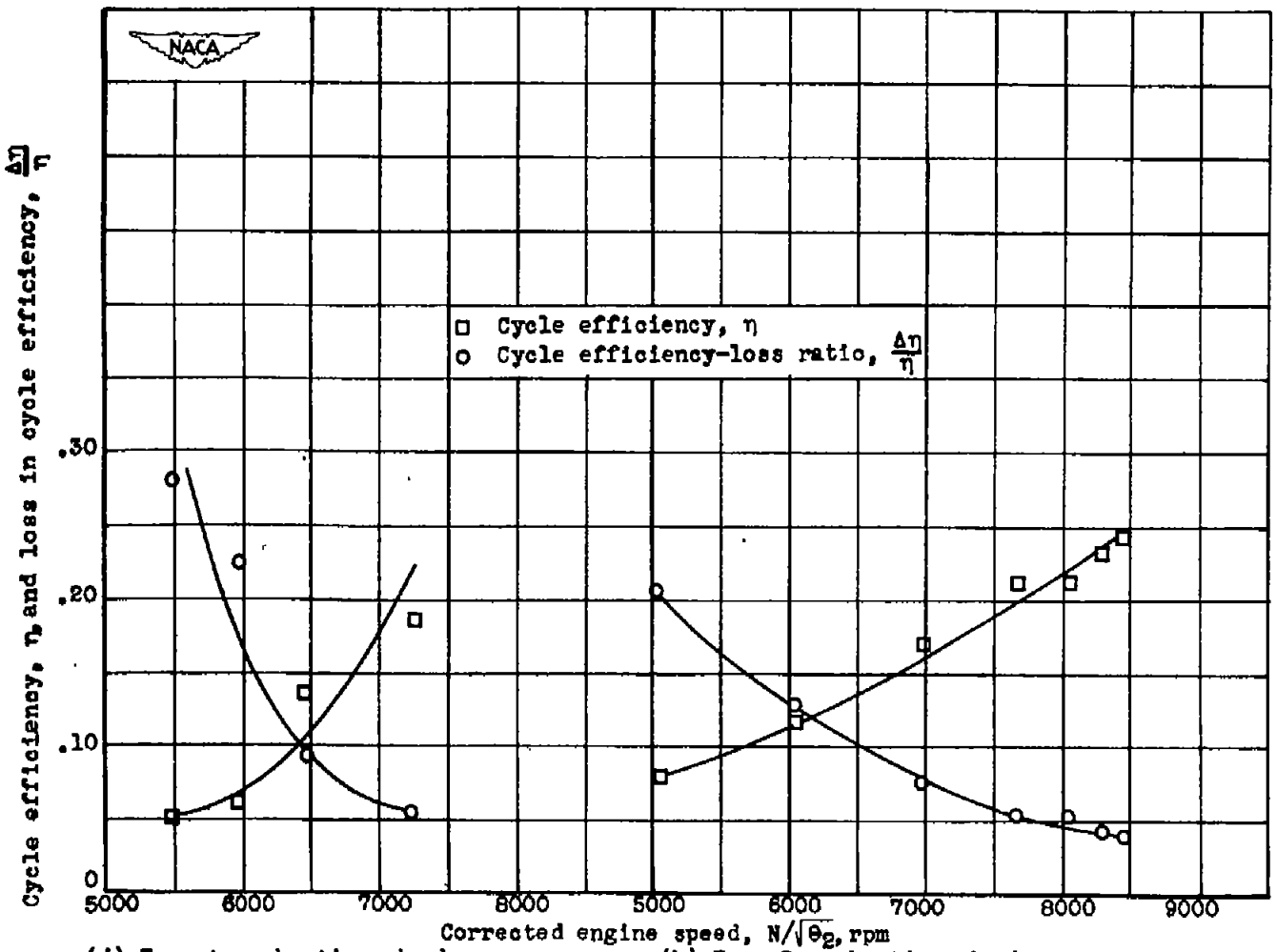

(j) Type A combustion chamber; pressure altitude, 40,000 feet; low-flow compressor; small turbine nozzle; $16\frac{1}{4}$-inch-diameter tail-pipe nozzle.

(k) Type B combustion chamber; pressure altitude, 40,000 feet; low-flow compressor; standard turbine nozzle; $16\frac{3}{4}$-inch-diameter tail-pipe nozzle.

Figure 11.- Concluded. Effect of altitude on loss in cycle efficiency due to combustion-chamber pressure losses. Static conditions.

654

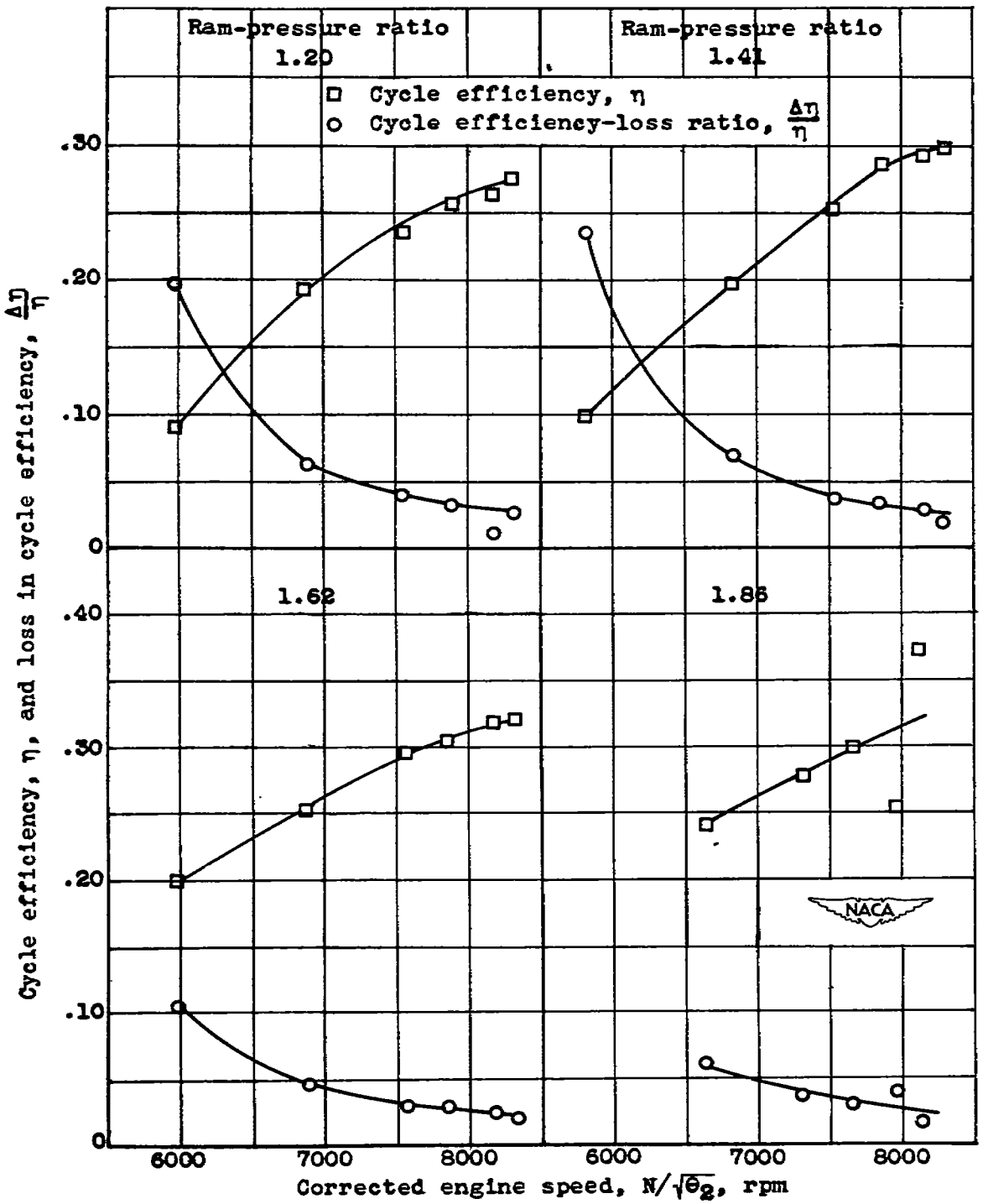

Figure 12.- Effect of ram pressure ratio on loss in cycle efficiency due to combustion-chamber pressure losses for type B combustion chamber. Pressure altitude, 40,000 feet; low-flow compressor; standard turbine nozzle; 16¾-inch-diameter tail-pipe nozzle.

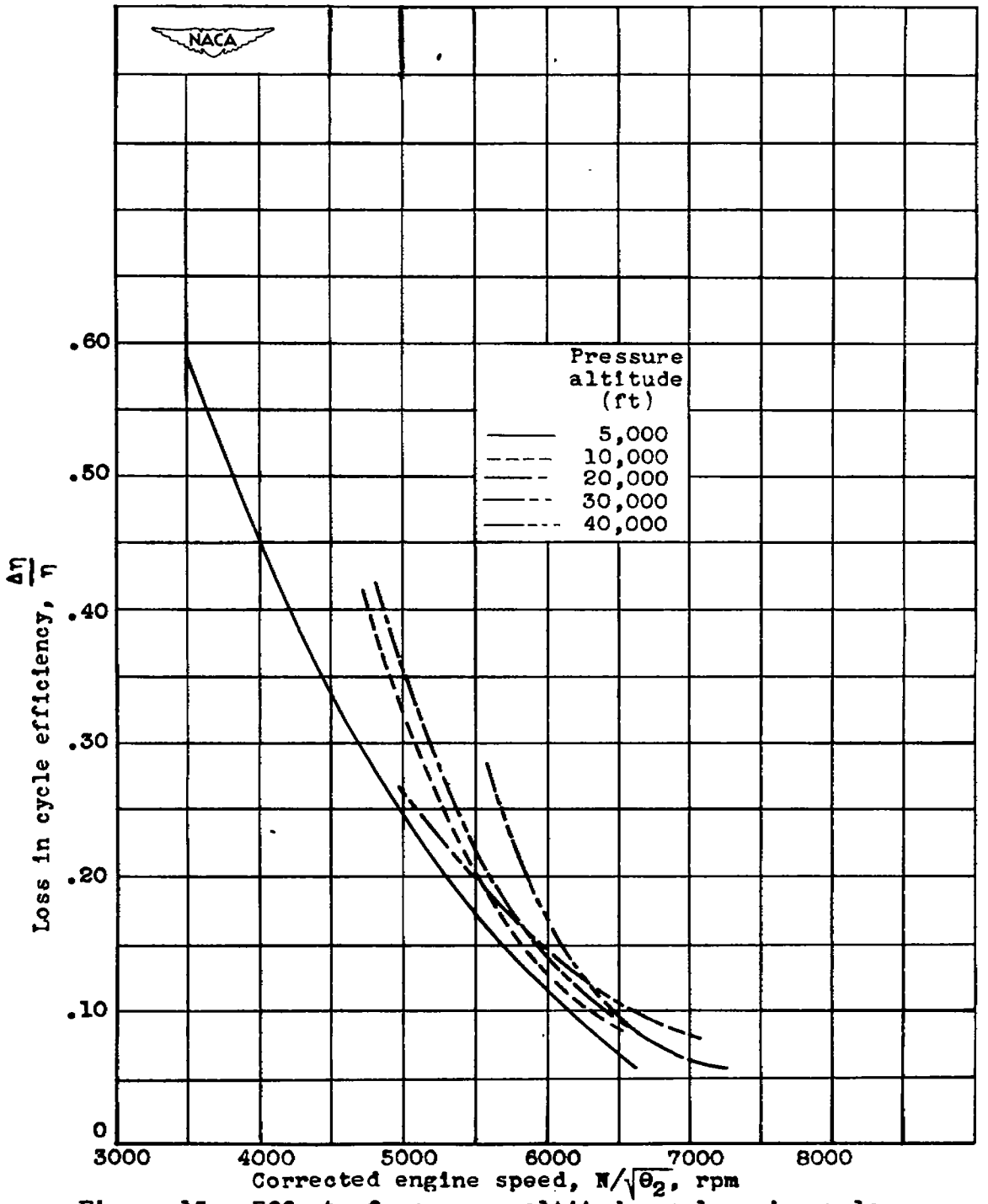

Figure 13.- Effect of pressure altitude on loss in cycle efficiency due to combustion-chamber pressure losses for type A combustion chamber. Static conditions; low-flow compressor; small turbine nozzle; $16\frac{1}{4}$-inch-diameter tail-pipe nozzle.

654

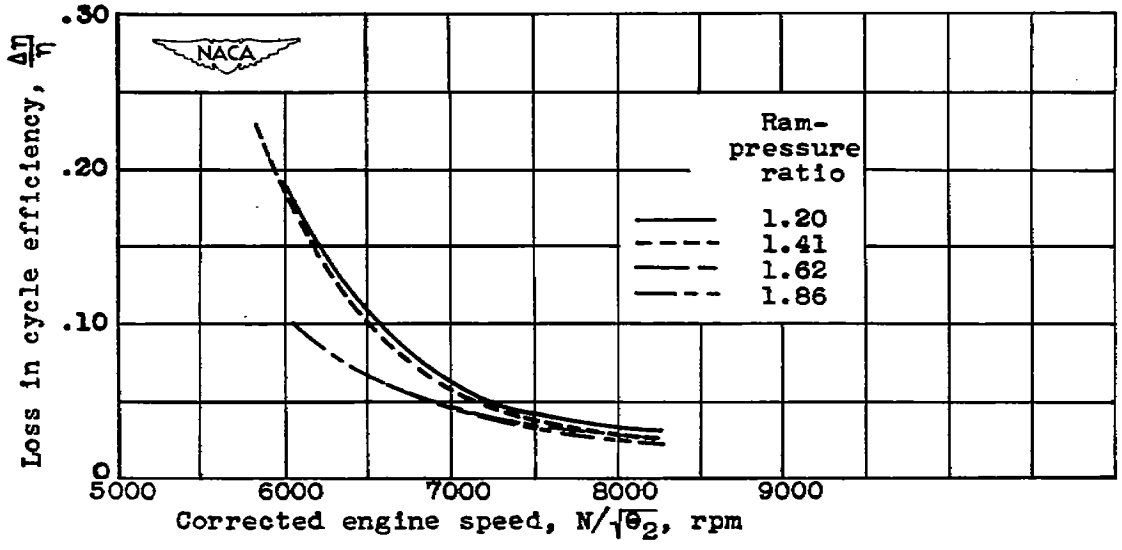

Figure 14.- Effect of ram-pressure ratio on loss in cycle efficiency due to combustion-chamber pressure losses for type B combustion chamber, cross plot from figure 12. Pressure altitude, 40,000 feet; low-flow compressor; standard turbine nozzle; $16\frac{3}{4}$-inch-diameter tail-pipe nozzle.

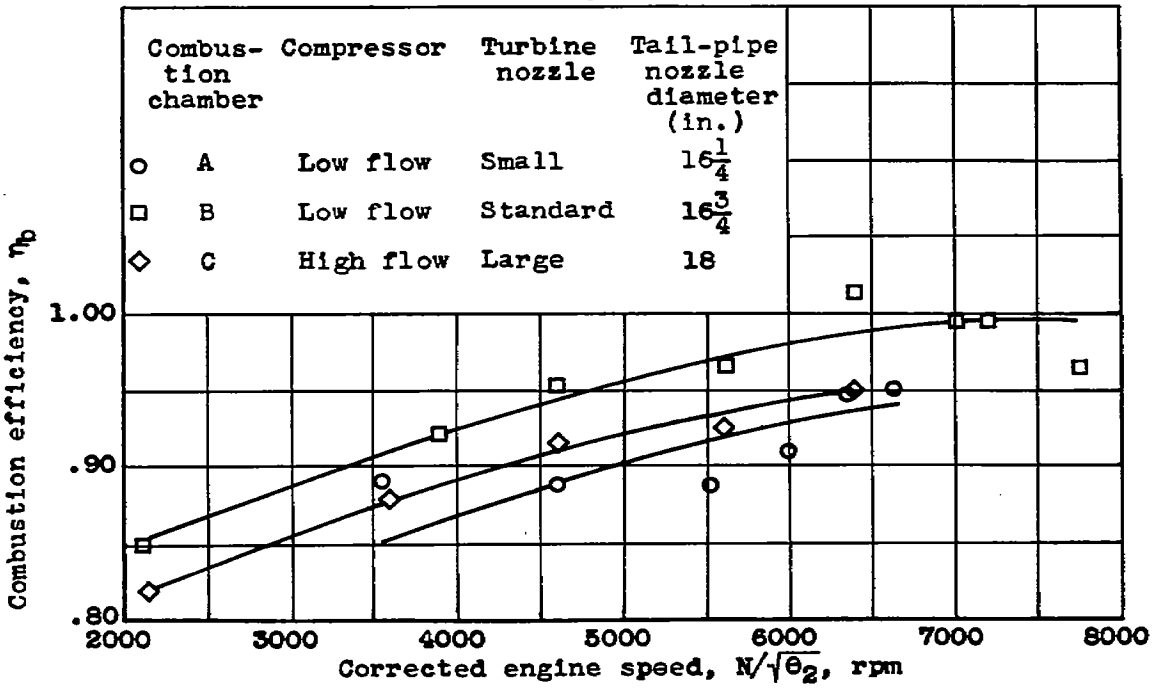

Figure 15.- Comparison of combustion efficiencies of types A, B, and C combustion chambers. Pressure altitude, 5000 feet; static conditions.

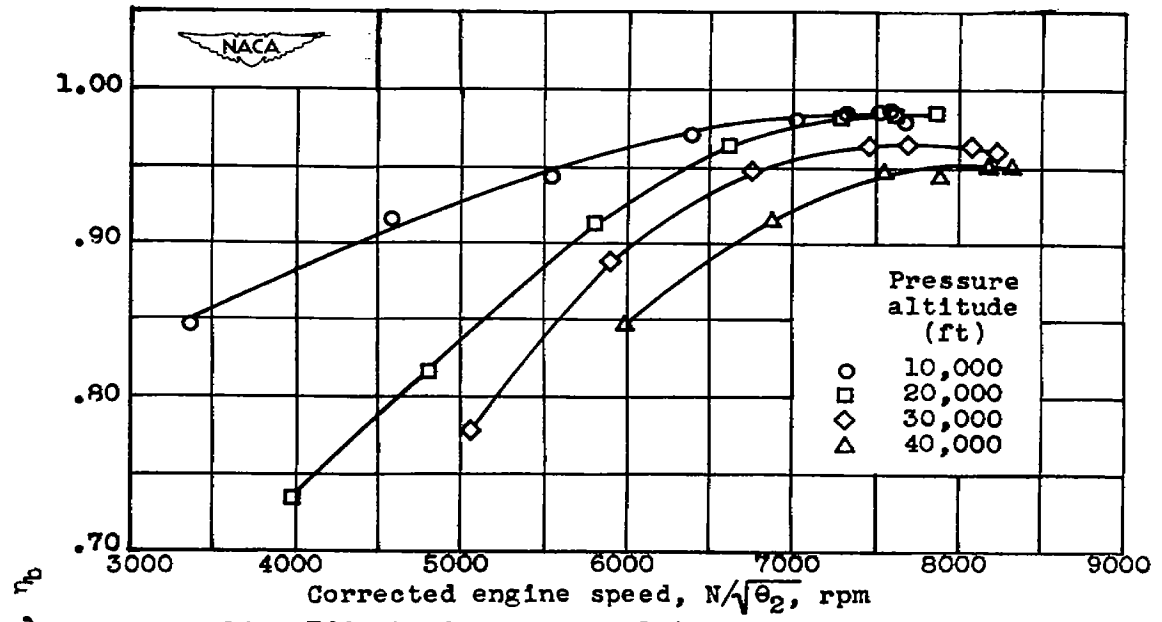

Figure 16.- Effect of pressure altitude on combustion efficiency for type B combustion chamber. Ram pressure ratio, 1.20; low-flow compressor; standard turbine nozzle; $16\frac{3}{4}$-inch-diameter tail-pipe nozzle.

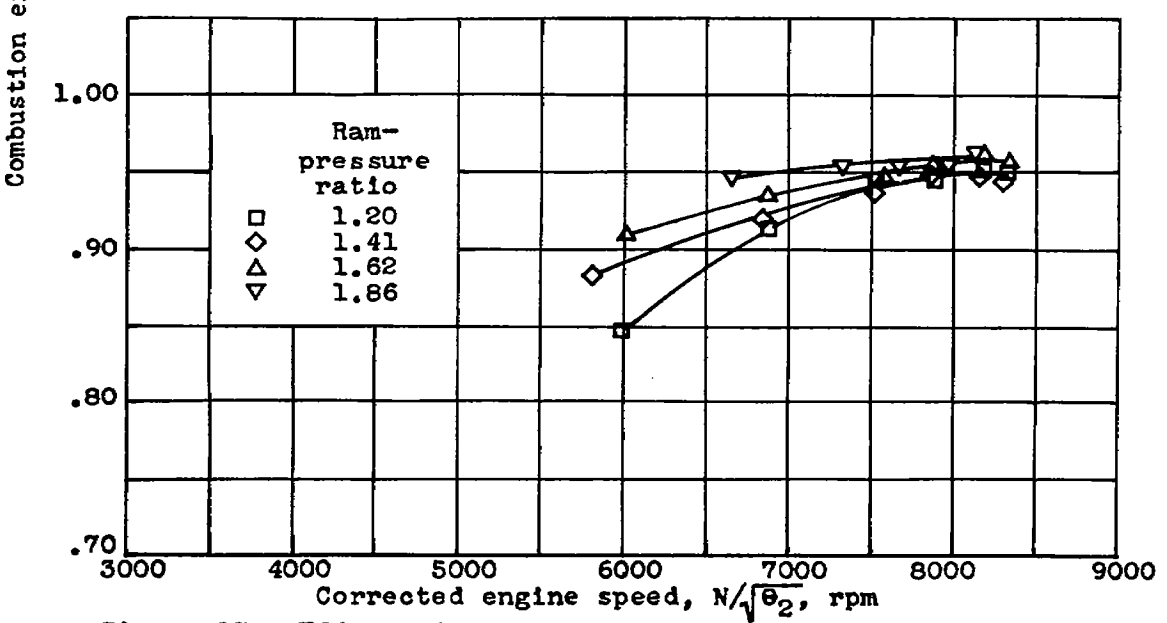

Figure 17.- Effect of ram pressure ratio on combustion efficiency for type B combustion chamber. Pressure altitude, 40,000 feet; low-flow compressor; standard turbine nozzle; $16\frac{3}{4}$-inch-diameter tail-pipe nozzle.

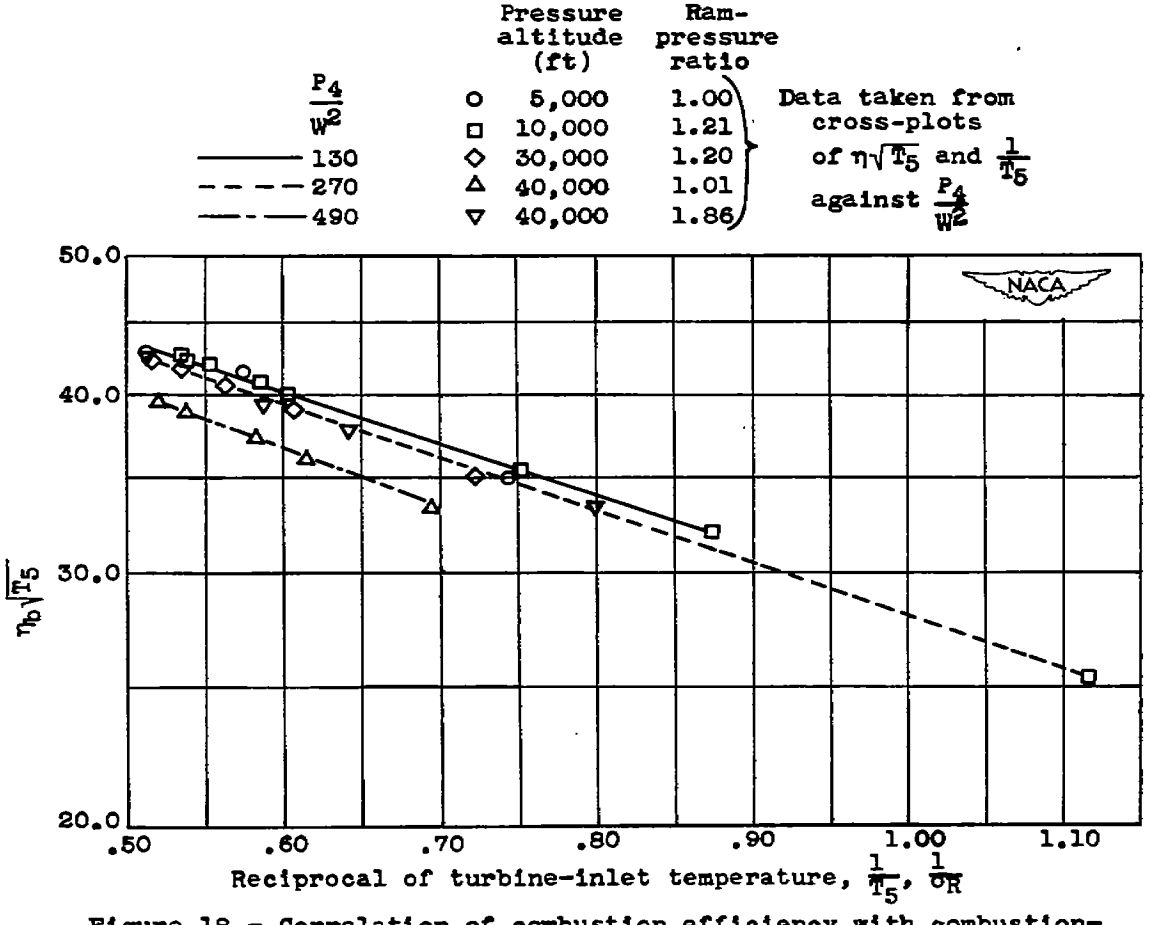

Figure 18.- Correlation of combustion efficiency with combustion-chamber-outlet temperatune for type B combustion chamber.

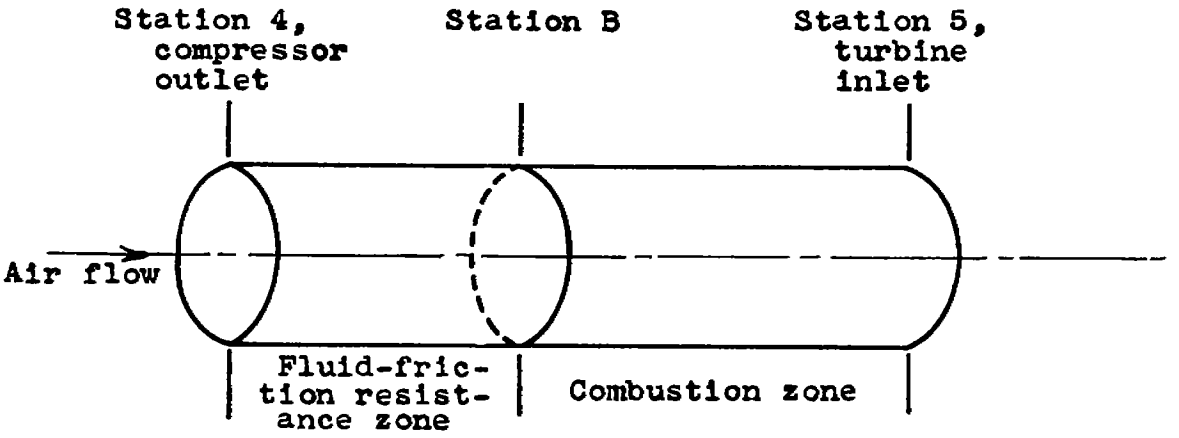

Figure 19.- Equivalent combustion chamber of constant cross section.

654

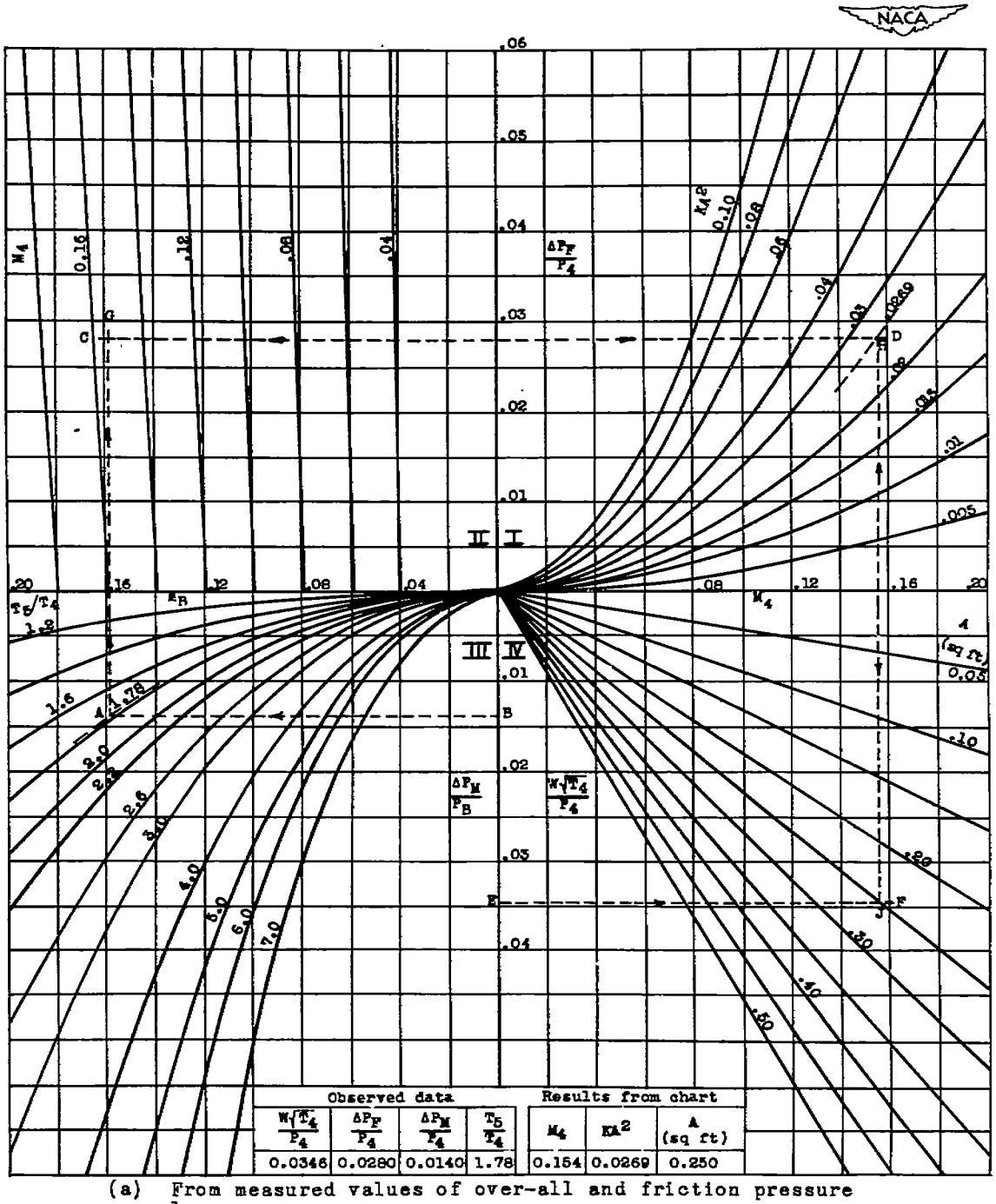

(a) From measured values of over-all and friction pressure losses.

Figure 20. - Determination of KA^2 and A for type B combustion chamber.

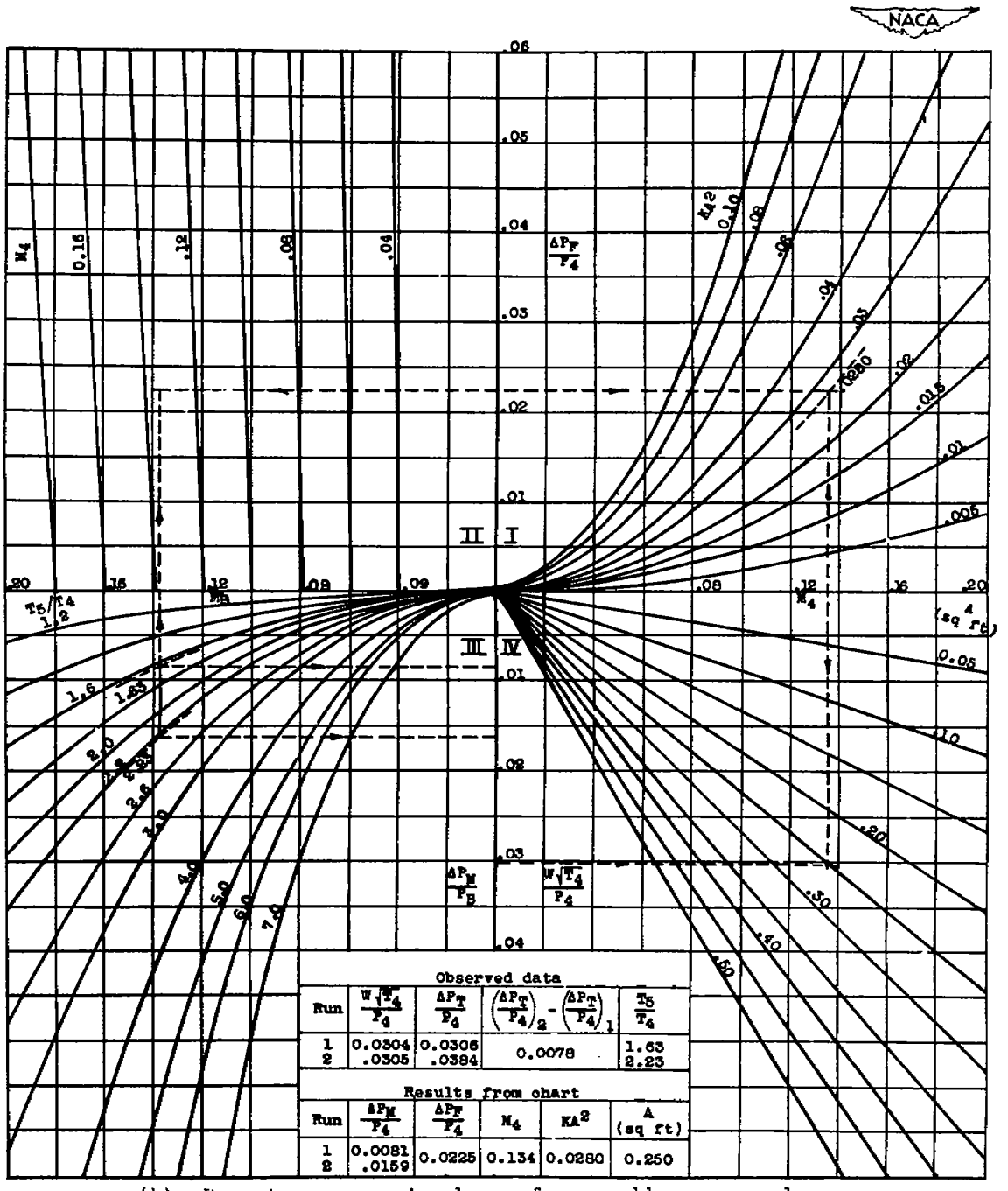

Observed data

Run	$\frac{W\sqrt{T_4}}{P_4}$	$\frac{\Delta P_T}{P_4}$	$\left(\frac{\Delta P_T}{P_4}\right)_2 - \left(\frac{\Delta P_T}{P_4}\right)_1$	$\frac{T_5}{T_4}$
1	0.0304	0.0306	0.0078	1.63
2	.0305	.0384		2.23

Results from chart

Run	$\frac{\Delta P_M}{P_4}$	$\frac{\Delta P_F}{P_4}$	M_4	KA^2	A (sq ft)
1	0.0081	0.0225	0.134	0.0280	0.250
2	.0159				

(b) From two measured values of over-all pressure loss.

Figure 20. - Concluded. Determination of KA^2 and A for type B combustion chamber.

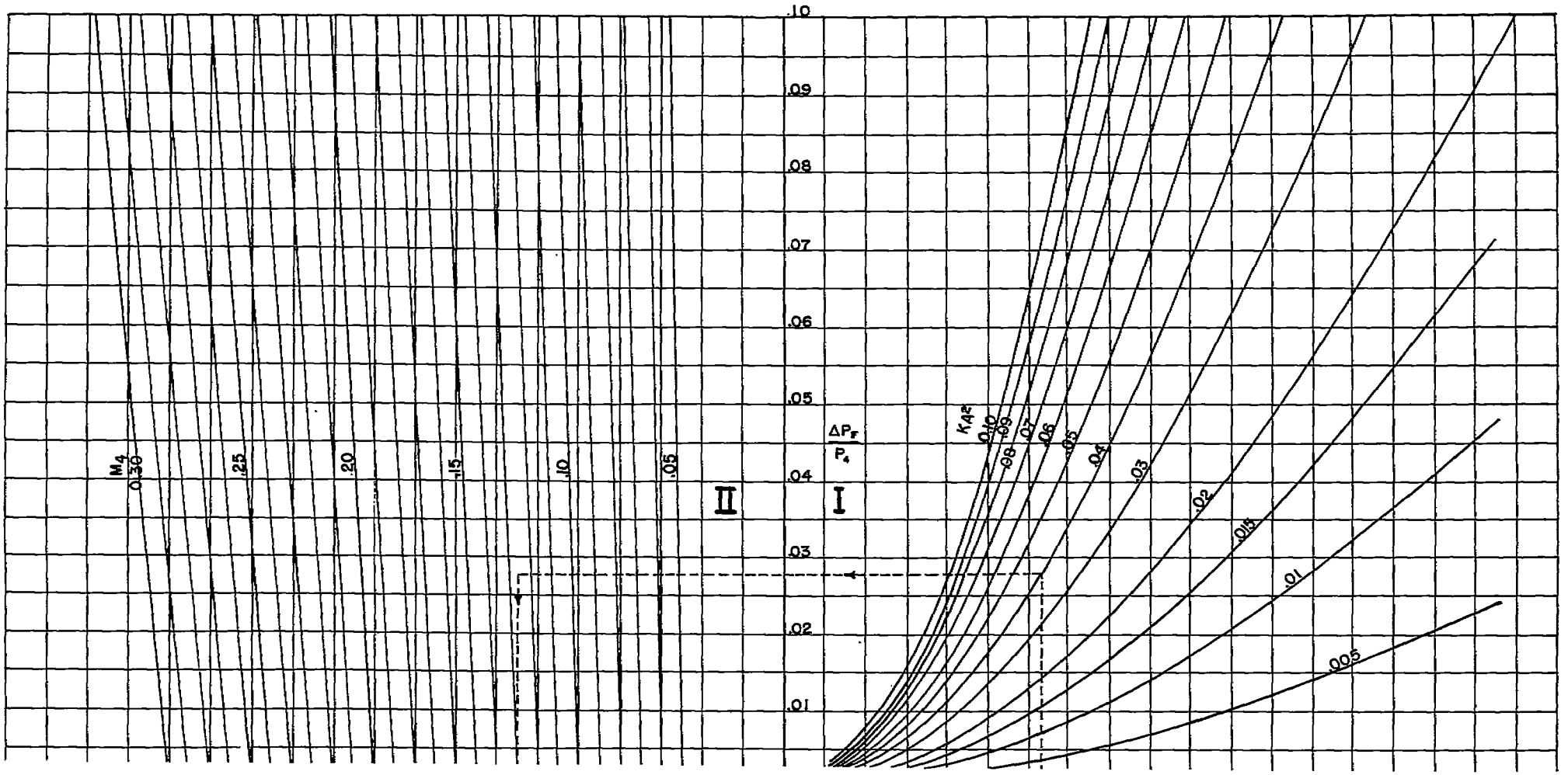
M_4
0.30
.25
.20
.15
.10
.05
II
I
$\frac{\Delta P_F}{P_4}$
K_{A^2}
0.10
.09
.08
.07
.06
.05
.04
.03
.02
.015
.01
.005
.10
.09
.08
.07
.06
.05
.04
.03
.02
.01

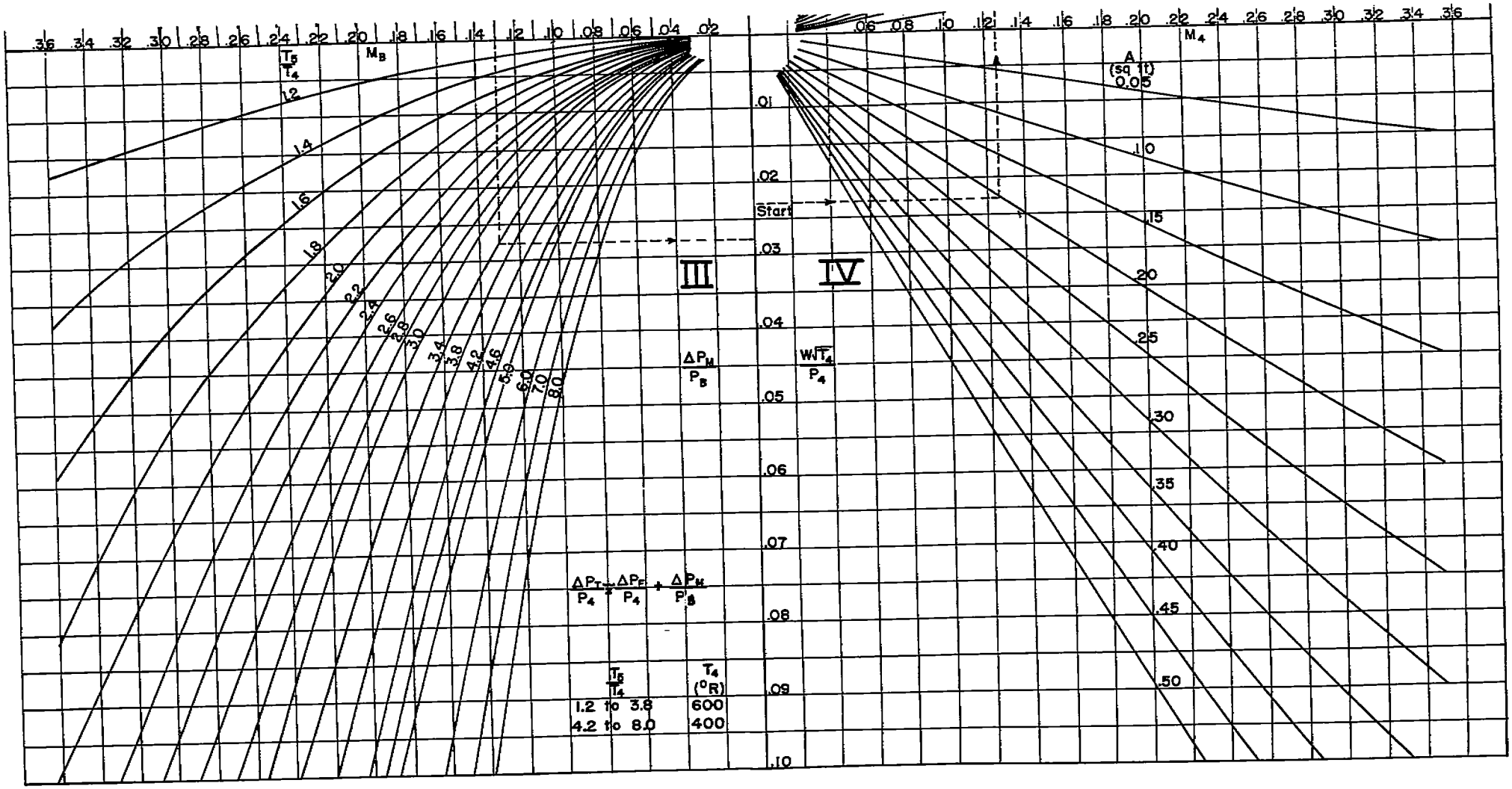

Figure 5.—Combustion-chamber pressure-loss chart.

NASA Technical Library
3 1176 01435 5367